ACS NANO

www.acsnano.org

ARTICLE

Aging of Self-Assembled Lead Halide Perovskite Nanocrystal Superlattices: Effects on Photoluminescence and Energy Transfer

Dmitry Baranov,* Antonio Fieramosca, Ruo Xi Yang, Laura Polimeno, Giovanni Lerario, Stefano Toso, Carlo Giansante, Milena De Giorgi, Liang Z. Tan,* Daniele Sanvitto,* and Liberato Manna*

Cite This: *ACS Nano* 2021, 15, 650−664

Read Online

ACCESS | Metrics & More | Article Recommendations | Supporting Information

ABSTRACT: **Excitonic coupling, electronic coupling, and cooperative interactions in self-assembled lead halide perovskite nanocrystals were reported to give rise to a red-shifted collective emission peak with accelerated dynamics. Here we report that similar spectroscopic features could appear as a result of the nanocrystal reactivity within the self-assembled superlattices. This is demonstrated by studying $CsPbBr_3$ nanocrystal superlattices over time with room-temperature and cryogenic micro-photoluminescence spectroscopy, X-ray diffraction, and electron microscopy. It is shown that a gradual contraction of the superlattices and subsequent coalescence of the nanocrystals occurs over several days of keeping such structures under vacuum. As a result, a narrow, low-energy emission peak is observed at 4 K with a concomitant shortening of the photoluminescence lifetime due to the energy transfer between nanocrystals. When exposed to air, self-assembled $CsPbBr_3$ nanocrystals develop bulk-like $CsPbBr_3$ particles on top of the superlattices. At 4 K, these particles produce a distribution of narrow, low-energy emission peaks with short lifetimes and excitation fluence-dependent, oscillatory decays. Overall, the aging of $CsPbBr_3$ nanocrystal assemblies dramatically alters their emission properties and that should not be overlooked when studying collective optoelectronic phenomena nor confused with superfluorescence effects.**

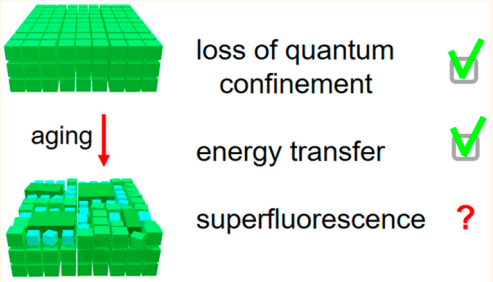

KEYWORDS: *perovskite nanocrystals, self-assembly, nanocrystal superlattices, environmental stability, reactivity, low-temperature photoluminescence, energy transfer*

Nanocrystals of lead halide perovskites are attractive and challenging materials in equal measure. On the one hand, $CsPbX_3$ (X = Cl, Br, and I) nanocrystals have a peculiar electronic structure,[1−3] which grants them defect-tolerance, ultrafast radiative decays,[4,5] and long exciton dephasing.[6] This combination of properties enables high-purity single-photon emission from individual nanocrystals[7−10] and makes them promising building blocks for nanocrystal solids to explore collective quantum phenomena that are challenging to achieve with other semiconductor nanocrystals. On the other hand, the dynamic surface chemistry of $CsPbX_3$ nanocrystals,[11−13] which promotes anion exchange, brings practical challenges such as nanocrystals degradation[14] and a loss of colloidal stability during the sample purification. This requires the development of innovative surface chemistries.[15−18] Apart from the single nanocrystals, colloids, and films, assemblies of $CsPbX_3$ nanocrystals (superlattices) are model systems which allow studying the properties of a nanocrystal ensemble with minimal size and shape distribution thanks to the selectivity of the self-assembly process.[19−21]

The superlattices of $CsPbBr_3$ nanocrystals have attracted attention in the past three years due to their collective optical and electronic properties.[22−30] In that short time span, a variety of quantum phenomena have been claimed in these materials, such as electronic coupling with the formation of minibands,[23] superfluorescence,[25,26] and low-threshold two-photon induced optical gain.[29] Therefore, $CsPbBr_3$ nanocrystal superlattices provide an exciting playground for the exploration of collective quantum phenomena. The straightforward fabrication of nanocrystal superlattices by self-assembly *via* slow solvent evaporation makes them readily available for experimentation. The $CsPbBr_3$ nanocrystals used for self-assembly in these studies are passivated with mixed (oleate and

Received: August 6, 2020
Accepted: December 7, 2020
Published: December 22, 2020

bromide)/(cesium and oleylammonium) ligand pairs[11,13] and are in a weak quantum confinement regime due to the ~9−11 nm size of the nanocrystals. In parallel with these developments, the progress in the synthesis of $CsPbBr_3$ nanocrystals enabled the fabrication of cesium oleate-capped shape-pure nanocubes with a smaller size and distinctly sharp excitonic absorption features,[31,32] which are better superlattice building blocks due to higher uniformity in their shape and stronger quantum confinement.

Regardless of the synthetic methods and surface passivation of $CsPbX_3$ nanocrystal building blocks, their dynamic chemistry makes nanocrystal assemblies metastable, as it has been documented in reports of coalescence and halide expulsion under external stimuli such as pressure,[33] heating,[34−36] or illumination.[37] Much less is known about the nanocrystal stability in superlattices under common sample handling conditions (*e.g.*, under vacuum or in the air) and its effect on the optical properties of individual superlattices. In this study, we fill this gap by correlating micro-photoluminescence (micro-PL) properties, morphology, and composition of pristine $CsPbBr_3$ nanocrystal superlattices (Figure 1), with those of vacuum- and air-exposed samples (Figures 2−4). It is observed that, under vacuum, $CsPbBr_3$ nanocrystal superlattices undergo contraction and subsequent coalescence, producing a heterogeneous mixture of nanocrystals and larger $CsPbBr_3$ nanoparticles embedded inside the superlattice (Figure 3). A narrow, red-shifted PL peak appears in the aged sample and grows over time (Figure 2). The spectral dynamics of this new peak were probed experimentally by transient spectrally resolved PL spectroscopy (Figure 6) and explained by Förster resonance electronic excitation transfer (FRET) theory[38,39] (Figure 7).

In contrast to samples kept under vacuum, exposing samples to air results in the formation of faceted bulk-like $CsPbBr_3$ particles on top of the superlattices (Figure 4). These faceted particles can be detected *via* scanning electron microscopy (SEM) or micro-PL imaging. At cryogenic temperatures, the emission from those large faceted particles appears as a narrower low-energy PL peak, with lifetime much shorter than that of the $CsPbBr_3$ nanocrystals (Figure 4). Moreover, fluence-dependent oscillating behavior is observed in the decay dynamics of large $CsPbBr_3$ nanoparticles that were produced by deliberately aging a toluene dispersion of $CsPbBr_3$ nanocrystals (Figure 5). The spectroscopic properties of such bulk-like $CsPbBr_3$ particles, arising from nanocrystal degradation, appear quite similar to those previously attributed to a cooperative emission (superfluorescence) from self-assembled $CsPbBr_3$ nanocrystals,[25,26] in spite of their different origins. Overall, the presented findings demonstrate that nanocrystal reactivity is a source of unusual emission features in assemblies of $CsPbBr_3$ nanocrystals and that reactivity must be taken into account when exploring collective optical properties. The results highlight the importance of seeking robust surface passivation strategies for metal halide perovskite nanocrystals in order to increase their stability while maintaining the size and shape uniformity required for self-assembly.

RESULTS AND DISCUSSION

Photoluminescence of $CsPbBr_3$ Nanocrystals in Dispersion and Pristine Superlattices at Room Temperature. The starting shape-pure cesium oleate-capped $CsPbBr_3$ nanocrystals were synthesized *via* benzoyl bromide injection into a mixture of cesium and lead oleates in the presence of didodecylamine, as detailed in Methods.[31] The nanocrystals isolated from the synthesis and dispersed in toluene show a structured absorption spectrum with the lowest energy peak at 2.515 eV (493 nm, Supporting Information Figure S1). In a dilute dispersion, the photoluminescence full width at half-maximum (fwhm) of the $CsPbBr_3$ nanocrystals sample is 88.8 meV (E_{max}^{PL} = 2.476 eV), comparable to the fwhm of single nanocrystals.[40,41] The sharp peaks in the absorption and PL spectra are consequences of the sample being free from other nanocrystal shapes.[31] The photoluminescence quantum yield of the as-synthesized nanocrystals was ~30%; such a modest value is attributed to the postsynthetic washing step involving ethyl acetate as an antisolvent.[31] The average edge length of the nanocrystals was estimated to be ≈8 nm on the basis of PL

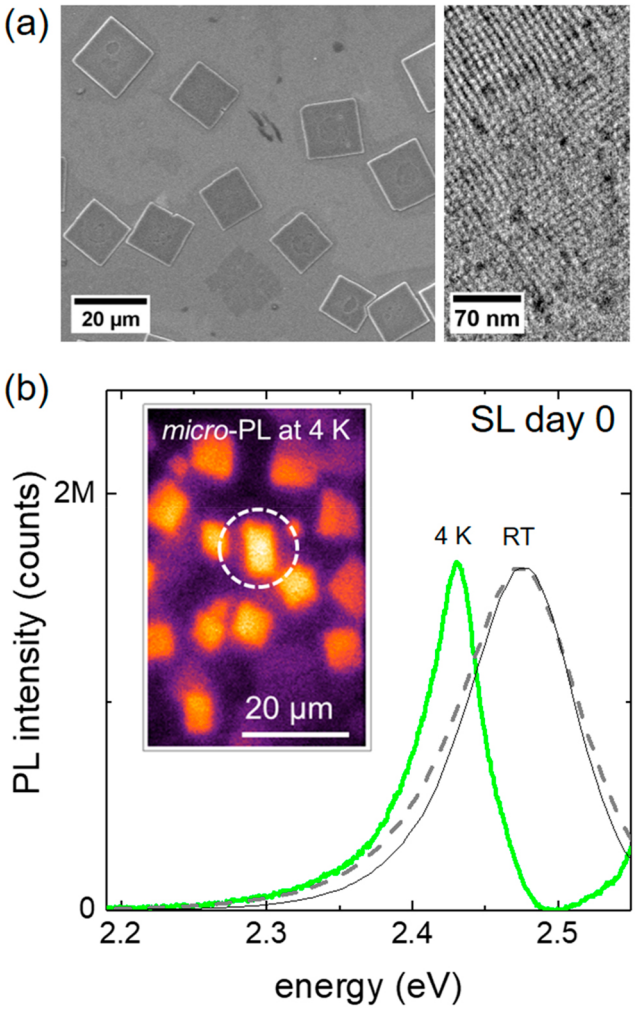

Figure 1. (a) Low- and high-magnification SEM images of a freshly made sample of $CsPbBr_3$ nanocrystal superlattices showing their micromorphology (left image) and closely packed individual nanocrystals on their surface (right image). (b) False-colored micro-PL image (inset, brightness represents PL intensity) and a cryogenic micro-PL spectrum (solid green line) collected from an individual $CsPbBr_3$ nanocrystal superlattice (circled in the inset) in a freshly made sample (SL day 0). The dashed gray line is a scaled room-temperature micro-PL spectrum of another superlattice from the same sample. The thin black line is a scaled PL spectrum of a dilute dispersion of $CsPbBr_3$ nanocrystals in toluene. The sample studied by micro-PL featured smaller superlattices than the sample imaged by SEM.

https://dx.doi.org/10.1021/acsnano.0c06595
ACS Nano 2021, 15, 650−664

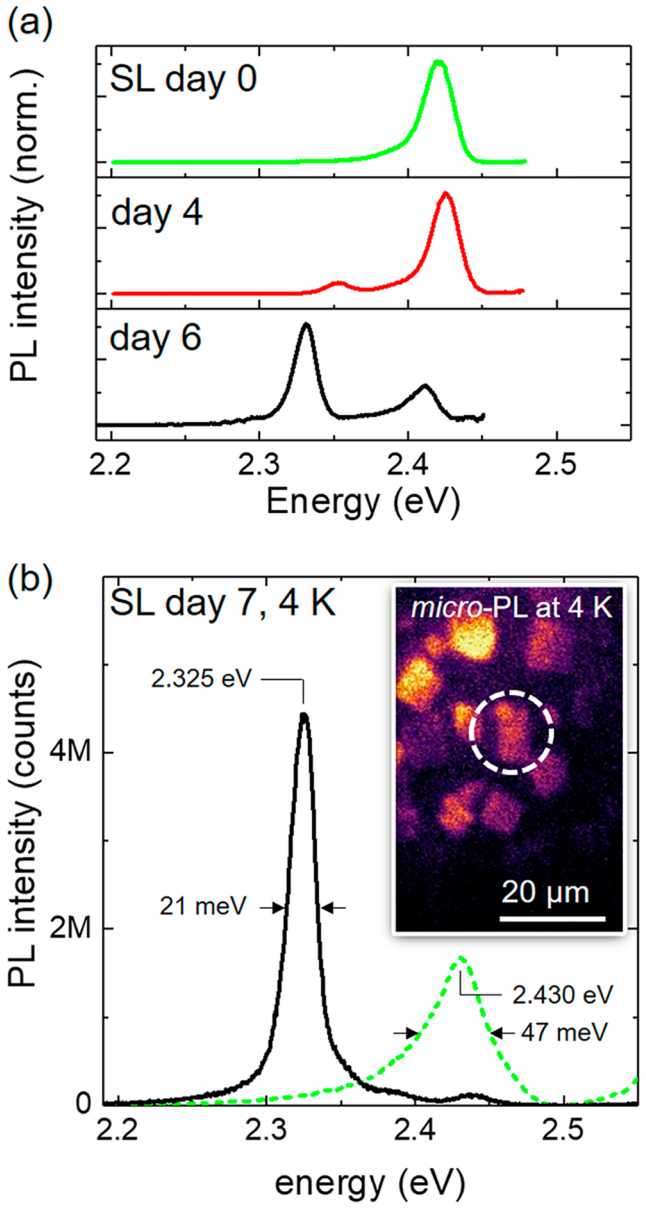

Figure 2. Cryogenic micro-PL spectra of individual $CsPbBr_3$ nanocrystal superlattices at various stages of aging. (a) micro-PL spectra of different superlattices from the same sample on days 0, 4, and 6 (green, red, and solid black curves, respectively). (b) micro-PL spectrum (black solid curve) and a false-colored micro-PL image (inset, brightness represents PL intensity) after 7 days. The green dashed curve is the micro-PL spectrum of the same superlattice collected on day 0 (and shown in Figure 1b).

and absorption maxima[42] and is consistent with the inspection of TEM images (Figure S2).

The self-assembly of nanocrystals was performed by solvent evaporation on the top of a squared Si wafer (see Methods). The resulting superlattices are flat rectangular objects composed of close-packed ≈8 nm $CsPbBr_3$ nanocrystals (Figure 1a) separated from each other by a ∼2 nm bilayer of cesium oleate surface capping species (one layer for each nanocrystal).[31] The room-temperature (295 K) PL spectra collected from five different superlattices were nearly superimposable (Figure 1b, gray dashed curve; Figure S3) with an average fwhm of 97.2 ± 2.7 meV and a E_{max}^{PL} ≈ 2.472 eV. Two changes in the room-temperature PL spectra of nanocrystals are evident when going from the dilute dispersion (Figure 1b, black solid curve) to the superlattice: a small red shift of the PL energy peak (Δ_E ≈ 4 meV) and a broadening (Δ_{fwhm} ≈ 9 meV).

In absorption, the spectral shifts to lower energies may be related to the changes in the dielectric environment when going from a dilute dispersion to a nanocrystal solid (*e.g.*, for CdSe,[43] CdTe,[44] and PbSe[45] nanocrystals). In PL, besides the dielectric effect, inter-nanocrystal energy transfer increases the shift to lower energies (*e.g.*, in CdSe[46,47] and CdTe[44] nanocrystal solids) as well as factors such as thickness-dependent self-absorption (inner filter effect)[33,48] and the presence of bulk-like impurities.[48] The small Δ_E ≈ 4 meV PL red shift of pristine superlattices and the spectrospatial homogeneity of the emission in micro-PL images (Figure S3) suggest that they are subject to minimal self-absorption and are free from impurities. A finite potential well calculation for a particle in an 8 nm box finds that the effective width of the ground state wave function is ≈8.39 nm (Figure S4; see Methods for the details of the calculations), which is smaller than the average superlattice periodicity of ≈10.2 nm (Figure 3b). Thus, the formation of minibands[23,30] is unlikely in these assemblies. The lack of a significant electronic coupling is an anticipated result if put in comparison with nanocrystal solids of metal chalcogenides,[49,50] which require a ligand exchange with short and conductive ligands[51] or an epitaxial connection between nanocrystals[52] to approach band-like electronic properties. On the other hand, recent reports on cooperative emission[25,26] suggest that a super-radiance effect could take place in such superlattices, giving rise to the significant spectral shifts.

Photoluminescence of Individual $CsPbBr_3$ Nanocrystal Superlattices at T = 4 K and Changes Caused by Aging in Vacuum. In order to understand the true nature of our observation, we performed a micro-PL study at cryogenic temperatures to investigate the light emission of individual superlattices. Upon cooling from room temperature to 4 K, the PL spectrum of single superlattices (Figure 1b, gray dashed curve) narrowed from fwhm = 92 to 47 meV and underwent a Δ_E = 44 meV shift to lower energy—a behavior typical of $CsPbBr_3$ perovskite in various dimensionalities (*i.e.*, bulk crystals, thin films, single nanocrystals, or nanocrystal films).[53−57] At 4 K, the PL spectrum (Figure 1b, solid green curve) consisted of a single asymmetric peak and did not show any additional lower energy peaks. The presence of a single peak was reproducibly observed on multiple superlattices grown from different nanocrystal batches (Figure S5). Upon warming the sample to room temperature, the individual superlattices developed cracks, and their rectangular shapes were distorted (Figure S6). Such morphological changes possibly stemmed from the evaporation of residual solvent molecules (trapped in the superlattices) under vacuum,[58] uniform thermal stress due to the contraction and expansion of the orthorhombic crystal structure of $CsPbBr_3$ perovskite nanocrystals,[59] or changes in the ligand packing.[60]

By aging the sample in vacuum at room temperature, we observed the appearance of a new peak at lower energies (Figure 2a). This new red-shifted PL peak became clearly distinguishable after ∼4 days of storage and kept growing and shifting in energy with aging time (Figure 2a and Figure S4). Virtually all of the PL signal in the sample arose from the low-energy peak after about a week, as demonstrated by the comparison between micro-PL spectra collected from the same

https://dx.doi.org/10.1021/acsnano.0c06595
ACS Nano 2021, 15, 650−664

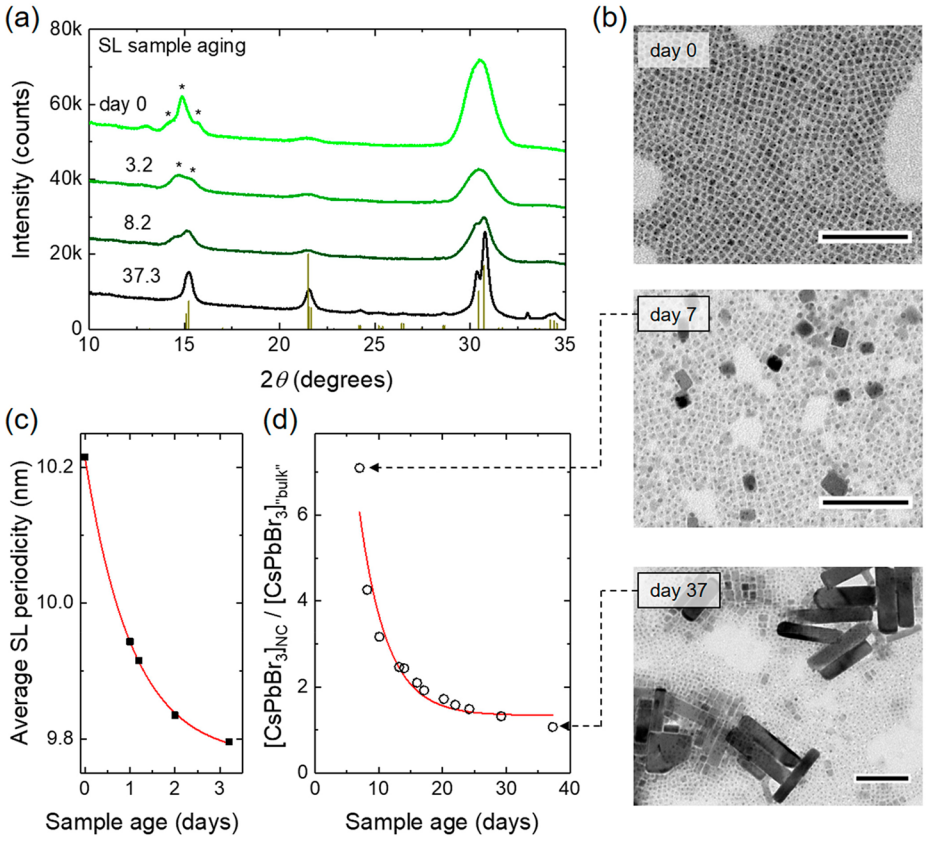

Figure 3. Aging of $CsPbBr_3$ nanocrystal superlattices as monitored by XRD and TEM. (a) XRD patterns of a superlattice sample aged in a vacuum for a different number of days. The superlattice reflections (marked by asterisks) decreased in intensity and disappeared over time, while the bulk-like reflections (stick pattern, orthorhombic $CsPbBr_3$, ID no. 96-451-0746, COD code 4510745)[65] began to dominate the signal. (b) TEM images of dissolved superlattices when fresh (day 0) and aged for a week (day 7) and for more than a month (day 37). The scale bar is 100 nm. (c, d) Plots showing the contraction of superlattice periodicity over the first 3 days and the coalescence expressed as the decrease in the nanocrystals to the "bulk" ratio obtained from the fit, respectively. The solid red lines in panels c and d are first-order kinetics fits with rate constants $k_{contraction} = 0.96 \pm 0.02$ and $k_{coalescence} = 0.23 \pm 0.04$ days^{-1}. The complete set of XRD patterns of the aging superlattice sample and an example of the fit are provided in Figure S13.

superlattice on the day of its preparation (day 0) and after 7 days of aging (Figure 2b). The magnitude of the aging-induced PL red shift was $\Delta_E \approx 105$ meV. The energy shift was accompanied by a ~55% peak narrowing, from fwhm of 47 to 21 meV. A comparison of the reflectance spectra of individual superlattices at $T = 4$ K revealed that the initial nanocrystals were still prominently present in the aged sample (Figure S7), even though most of the PL intensity (~96% by area) was contained in the lower energy peak. Measurements of the first-order temporal coherence (Figure S8) revealed a longer coherence time of ≈150 fs for the low-energy peak compared to ≈70 fs for the high-energy peak, an increase very similar to that reported for coupled nanocrystals in superfluorescent assemblies.[25] However, an inspection of the second-order temporal coherence on a few nanocrystal superlattices found no superbunching effect.

The energy position, line width, and dynamics of the newly formed low-energy PL peak (at cryogenic and room temperatures) are interpreted as a loss of quantum confinement[61,62] and a result of inter-nanocrystal energy transfer. First, both energy position and line width are very similar to the PL of bulk-like $CsPbBr_3$ perovskite compounds.[57,63−65] The gradual appearance and growth of the low-energy PL peak over time is compatible with the spontaneous fusion of nanocrystals while the sample is stored in vacuum at room temperature. To test this hypothesis, a replica sample of $CsPbBr_3$ nanocrystal superlattices was prepared and aged under vacuum for several days. Comparison of TEM images of nanocrystals from fresh and aged superlattices (prepared by dissolving superlattices in toluene) revealed the presence of large, ≈20−40 nm $CsPbBr_3$ particles after 7 days of aging (Figure S9), confirming that nanocrystal sintering occurred in the sample. Unsurprisingly, both absorbance and PL spectra of the dissolved aged superlattices were broadened and shifted to lower energies if compared to the freshly made nanocrystals (Figure S10). High-resolution SEM of the 7 day old superlattices in cross-section also indicated the presence of bright spots scattered across the superlattice (Figure S11), which are interpreted as large $CsPbBr_3$ inclusions distributed throughout the aged superlattice.

Second, these interpretations are supported by theoretical calculations of quantum confinement in lead halide perovskite nanocrystals.[66] As the nanocrystal diameter is increased from 6 to 12 nm, our models predict a PL red shift of 90 meV (Figure S12), comparable to the measured PL red shift of 105 meV. The experimentally observed sharpening of the PL spectrum during aging (Figure 2b) is a result of the band gap's reduced sensitivity to nanocrystal size when nanocrystals are large. A simulation comparing normal distributions of small (5 nm) and large (9 nm) nanocrystals, both with a standard deviation

https://dx.doi.org/10.1021/acsnano.0c06595
ACS Nano 2021, 15, 650−664

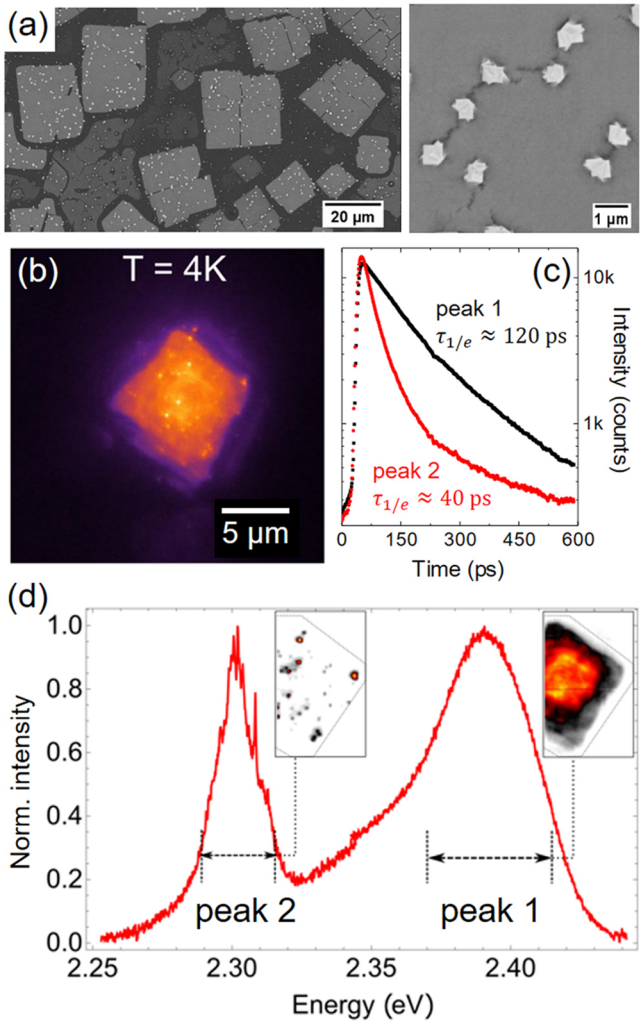

Figure 4. Effects of air exposure on individual $CsPbBr_3$ nanocrystal superlattices. (a) Low- and high-magnification SEM images showing superlattices covered with bright, faceted spots of bulk-like $CsPbBr_3$ particles. (b) False-colored micro-PL image of an individual superlattice at T = 4 K showing brightly emissive spots on its surface. (c) PL intensity decays of emission from high-energy and low-energy peaks (peaks 1 and 2, respectively) originating from the bulk of the superlattice and bright spots, respectively, as illustrated in (d) spectrally filtered micro-PL maps of the superlattice (insets).

of 1 nm, finds fwhm of 149 and 14 meV, respectively, qualitatively accounting for the narrowing of the PL spectra as the nanocrystal size increases (Figure S12). Furthermore, as a result of the nonlinear dependence of the band gap on the nanocrystal diameter, the PL line shape of the simulated 5 nm ensemble of nanocrystals is predicted to be asymmetric compared to that of 9 nm nanocrystals (Figure S12), which is consistent with the experimental data.

Previously, multiple reports have documented the propensity of $CsPbX_3$ nanocrystals to coalesce under external stimuli such as light[67−69] or heat,[34−36,70,71] from the destabilizing action of polar solvents,[72−74] or spontaneously due to aging in dispersion[75] or on a solid substrate.[76] To gain insight into the transformations of $CsPbBr_3$ nanocrystals as they age in a vacuum, a series of wide-angle XRD patterns were collected from the sample stored under medium vacuum (∼0.4−0.7 mbar) at room temperature for more than a month. The XRD patterns collected at days 0, 3.2, 8.2, and 37.3 are shown in Figure 3a along with TEM images of fresh, 7, and 37 days old dissolved nanocrystal superlattices in Figure 3b. The TEM images reveal the presence of large $CsPbBr_3$ nanocrystals that grow over time. The fine structure of the peak at $2\theta \sim 15°$ in the fresh sample (Figure 3a, day 0) contains information about the average superlattice periodicity,[37,58,77] which is estimated to be ≈10.2 nm (consistent with a sum of the nanocrystal edge length, ≈8.0 nm, and interparticle spacing, ≈2.2 nm). The position of the most intense superlattice fringe shifts to a higher angle over time, which is interpreted as the contraction of the average superlattice periodicity from ≈10.2 to ≈9.8 nm (Figure 3c). The breaking of the superlattice into smaller subdomains of random orientations is unlikely at that stage as it would result in the disappearance of the superlattice fringes and broadening of the peak, which were not observed. The uniform contraction of the superlattice into a nanocrystal solid with near-zero interparticle spacing is also unlikely to have occurred, as it would push the superlattice fringes apart (reflecting decreased interparticle spacing) but preserve the breadth of their envelope, due to the size-broadening. Instead, a narrowing of the diffraction peaks is observed over time. The peak at $2\theta \sim 30°$ (arising from the (004) and (220) reflections of the orthorhombic $CsPbBr_3$ perovskite crystal structure) underwent an initial drop in intensity (Figure 3a, day 0 to day 3.2); then it narrowed and split into two components (Figure 3a, days 8.2 and 37.3). The complex shape of this peak was fit to a sum of three Gaussians representing the single broad nanocrystal and the twin sharp bulk-like contributions (Figure S13). The changes in the ratio between the integrated areas of the fitted nanocrystal ($[CsPbBr_3]_{NC}$) and the bulk-like peaks ($[CsPbBr_3]_{bulk\text{-}like}$) were exploited to track the coalescence evolution over time, as shown in Figure 3d. The time dependence of both the contraction and the coalescence was fit to simple first-order kinetics (Figure 3c,d, solid red curves) with rate constants of $k_{contraction} = 0.96 \pm 0.02$ and $k_{coalescence} = 0.23 \pm 0.04$ days^{-1}. The first-order kinetics was used in analogy with a prior report of heat-induced coalescence of $CsPbBr_3$ nanocrystals.[70] The overall picture is that the superlattice contracted primarily during the initial period of 3 days, followed by a slow coalescence into large crystalline domains that continued for over a month.

Changes in Photoluminescence Spectra Caused by Aging in Air. Unlike self-assembled metal and metal chalcogenide nanocrystals, the $CsPbBr_3$ nanocrystals react readily with air and moisture to form faceted bulk-like $CsPbBr_3$ particles on top of the superlattices. At room temperature, the detection of these bulk-like particles required an inspection by SEM (Figure 4a), where they appeared as high-contrast objects, or a micro-PL, where they appeared as bright spots with red-shifted emission (Figure S14). At 4 K, the bulk-like $CsPbBr_3$ particles contributed with a narrow, low-energy peak ($E^{PL}_{max} \sim 2.30$ eV; fwhm ∼ 17 meV) carrying sharp spikes, as revealed by spectrally filtered micro-PL images (peak 2, Figure 4b−d). The superlattices in the sample were affected by the air exposure heterogeneously, resulting in varying coverage of superlattices with bright spots and different PL spectra (Figure S15). The PL intensity decay of the low-energy peak was significantly faster ($\tau_{1/e}$∼ 40 ps, peak 2 in Figure 4c) than that of the rest of the superlattice ($\tau_{1/e} \sim 120$ ps, peak 1 in Figure 4c). Initial observations of the energy position and accelerated dynamics, as well as the increase of temporal coherence of peak 2, suggested superfluorescent emission, but several attempts to

https://dx.doi.org/10.1021/acsnano.0c06595
ACS Nano 2021, 15, 650−664

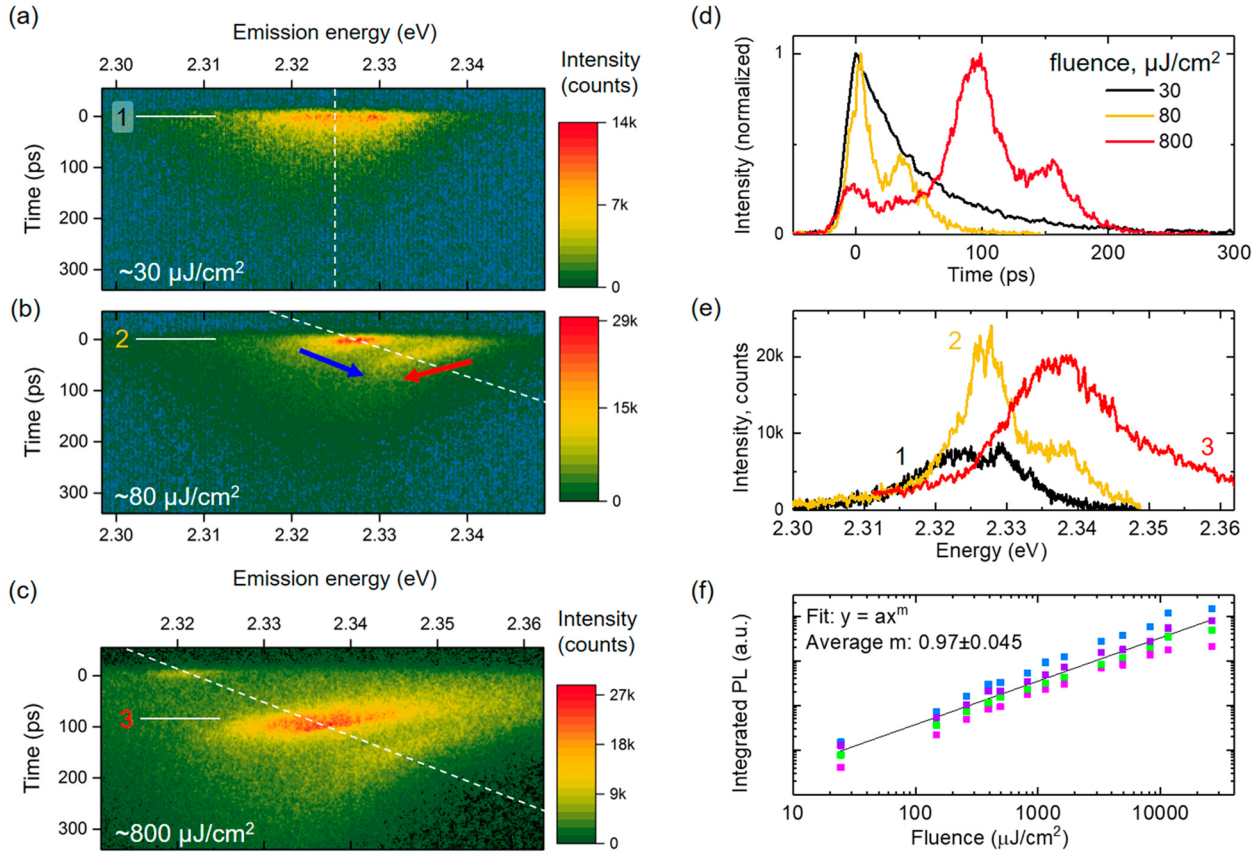

Figure 5. PL of bulk-like $CsPbBr_3$ particles at T = 4 K in the absence of superlattices. (a–c) Streak camera images of the PL decays at the excitation fluences of ~30, ~80, and ~800 $\mu J/cm^2$ (λ_{exc} = 470 nm, ~50 fs pulse duration, 10 kHz repetition rate). The color-coded PL intensity is plotted on a log scale. A progression of narrow emission peaks appears with increasing excitation power. Each individual peak shifts toward lower energy with time, while the progression of peaks builds up toward higher energy, as highlighted by red and blue arrows in panel b. (d) PL intensity decay slices showing the oscillatory behavior. The slices were taken along the direction shown by white dashed lines, which are tilted in panels c and b because they go through the maxima of the oscillating peaks. At the lowest fluence, $\tau_{1/e} \approx 50$ ps, and it accelerates as the fluence increases. Up to three peaks are discernible at the highest excitation fluence of ~800 $\mu J/cm^2$. (e) Spectral slices through the maximum intensity peaks revealing a substructure of sharp spikes on top of the broader PL spectrum. The slices were taken horizontally along the narrow regions of interest indicated by white solid lines and numbered 1–3. (f) Integrated PL intensity *vs* excitation fluence for four different regions in the sample of bulk-like $CsPbBr_3$ particles with an average power law fit (black thin line) with an exponent of 0.97 ± 0.045. Fits for each region and a complete series of fluence-dependent spectra are provided in Figure S21.

measure second-order temporal coherence revealed no bunching effects (see Methods and Figure S16). That discrepancy prompted us to focus on the bulk-like $CsPbBr_3$ particles as sources of the unusual low-energy emission. The formation of bulk-like particles on top of the superlattices is indicative of the $CsPbBr_3$ nanocrystals reactivity with air. Thus, it is reasonable to anticipate that the formation of bulk-like $CsPbBr_3$ particles would also occur in dispersion, where they could be isolated and characterized without superlattices around them.

To explore this approach, a toluene dispersion of as-synthesized ≈8 nm $CsPbBr_3$ nanocrystals was left under air for 3 days, producing a yellow-white precipitate consisting of a mixture of 10s–100s nm $CsPbBr_3$ and Pb(OH)Br (laurionite structure)[78−80] particles, which was identified by a combination of XRD and energy-dispersive X-ray spectroscopy in high-resolution SEM (Figure S17). The formation of Pb(OH)Br is rationalized by the perovskite hydrolysis in the presence of moisture: $2CsPbBr_3 + H_2O \rightarrow CsPbBr_3 + Pb(OH)Br + HBr + CsBr$. The growth of bulk-like $CsPbBr_3$ particles is possibly a result of HBr-catalyzed dissolution–recrystallization of the initial nanocrystals. The XRD patterns did not contain evidence of crystalline CsBr, despite its formation being required to balance the hydrolysis. The lack of crystalline CsBr could be explained by either its subsequent hydrolysis or solvation of Cs^+ and Br^- ions by organic species. Hydrolysis is an unusual transformation in assemblies of semiconductor nanocrystals and is different from the previously documented instances of reactivity during self-assembly of nanocrystals, such as precipitation of selenium crystals due to the residual precursor in the case of CdSe nanocrystals.[81−83]

The ability to produce bulk-like $CsPbBr_3$ particles from nanocrystals enables the examination of their PL properties in the absence of nanocrystal superlattices. At room temperature, a sample of bulk-like $CsPbBr_3$ particles exhibits narrow emission spikes above a ~3 mJ/cm^2 threshold and that was interpreted as random lasing (Figure S18). When cooled to T = 4 K, a dilute sample of bulk-like $CsPbBr_3$ particles shows a variety of sharp PL peaks ($E^{max}_{bulk\text{-}like}$ ~ 2.29–2.35 eV, Figure S19) with short lifetimes ($\tau_{1/e}$ ~ 50 ps) at relatively low excitation fluence (~30 $\mu J/cm^2$, Figure 5a). At higher fluences, the PL decays accelerate and develop an oscillatory decay that consists of a progression of short peaks, with up to three consecutive peaks distinguishable at the highest applied fluence

https://dx.doi.org/10.1021/acsnano.0c06595
ACS Nano 2021, 15, 650–664

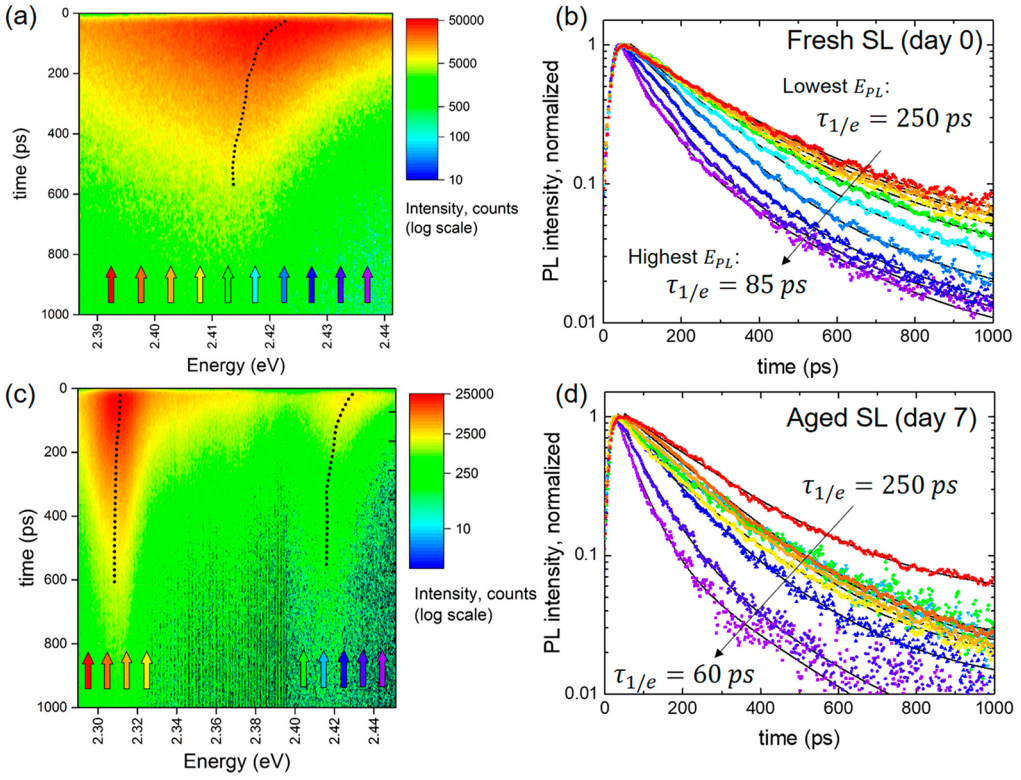

Figure 6. Time- and energy-resolved PL of individual superlattices in a fresh (a, b) and aged (c, d) sample. Streak images (a, c) and normalized PL decays (b, d) at various energy positions as indicated by the colors of the decay curves and arrows in panels a and c. The sample was excited with a pulsed femtosecond laser (λ_{exc} = 470 nm, ~50 fs pulse duration, 10 kHz repetition rate) and incident fluences of ~10 and ~25 μJ/cm^2 for fresh and aged superlattices, respectively. The black dotted line in panels a and c tracks the PL peak energy position over time. The solid black lines in panels b and d are the fits to the data.

of ~800 μJ/cm^2 (Figure 5b–d; see Figure S20 for spectrally resolved PL decays in different regions of the sample). Each individual peak shifts toward lower energy with time, while the progression of peaks builds up in the direction of higher energy, as indicated by red and blue arrows in Figure 5b. The period of the oscillations increases with fluence, instead of accelerating as it would be expected from an idealized Burnham–Chiao ringing of superfluorescence.[84] The narrow spikes are noticeable at early decay times in spectral slices at different fluences (Figure 5e) as well as in the integrated PL spectra beginning from the lowest fluence of ~25–30 μJ/cm^2 (Figures S19 and S21). The spikes demonstrate a significantly lowered lasing threshold at 4 K as compared to room temperature. The integrated PL intensity dependence *vs* fluence measured at 4 K for that sample follows a power law with an average exponent of 0.97 ± 0.045 (Figure 5f and Figure S21) and is suggestive of radiative recombination of excitons.[85] The progression of short peaks that display similar dynamics in energy and time have been observed in $CsPbBr_3$[85,86] and ZnO[87,88] nanomaterials pumped above the lasing threshold and are assigned to stimulated emission from an electron–hole plasma. We attribute the fluence-dependent oscillations in bulk-like $CsPbBr_3$ particles at 4 K to the same phenomenon. In addition, the sharp peaks observed in the PL spectra of nanocrystal superlattices aged in air (Figure 4d, Figure S15d) can be assigned to emission from the bulk-like $CsPbBr_3$ particles enhanced by the energy transfer from the rest of the superlattice, which we discuss in detail below.

Comparison with Superfluorescence. The optical properties of aged superlattices and bulk-like $CsPbBr_3$ particles studied in this work closely resemble the spectral signatures of superfluorescence reported from superlattices of ~9.5 nm $CsPbBr_3$ nanocrystals where aging was not considered.[25] The similarities of the superfluorescence (SF) reported in ref 25 and red-shifted emission due to aging are (1) the energy peak position, E^{SF}_{max} ~ 2.31 eV *vs* 2.29–2.35 eV for the aged samples; (2) narrow $fwhm_{SF}$ = 15 ± 4 meV *vs* 17–21 meV (and narrower for stimulated emission spikes) for the aged samples; (3) accelerated dynamics, τ_{SF} = 14 ps at ~1.2 mJ/cm^2 *vs* 40–50 ps at low fluence or shorter at high fluence for aged samples; (4) oscillating emission decays appearing as a progression of peaks for the SF and bulk-like $CsPbBr_3$ particles under increased excitation fluence; (5) the integrated PL intensity dependence of the SF *vs* fluence exhibits a power law with an exponent of ≈1 *vs* 0.97 ± 0.045 for the emission from bulk-like $CsPbBr_3$ particles; (6) increased first-order temporal coherence time from <40 to 140 fs for the SF emission *vs* from 70 to 150 fs for the superlattices aged in vacuum. The differences between materials and observations of this study and the superfluorescent ones of ref 25 are (1) this study uses smaller $CsPbBr_3$ nanocrystals (~8 nm) derived from a different synthesis; (2) the peak PL amplitude of the oscillating decays for bulk-like $CsPbBr_3$ particles does not show superlinear dependence *vs* excitation fluence while the peak PL amplitude of superfluorescent oscillations followed a power law with an exponent of 1.5 ± 0.1; (3) we did not observe a bunching behavior in the second-order coherence for the superlattices aged in vacuum and in air. The lack of real space PL images and spectra of the exact superfluorescent domains that showed bunching [$g^{(2)}(\tau) \sim 1.1$ and >2 in ref 25] prevents

https://dx.doi.org/10.1021/acsnano.0c06595
ACS Nano 2021, 15, 650–664

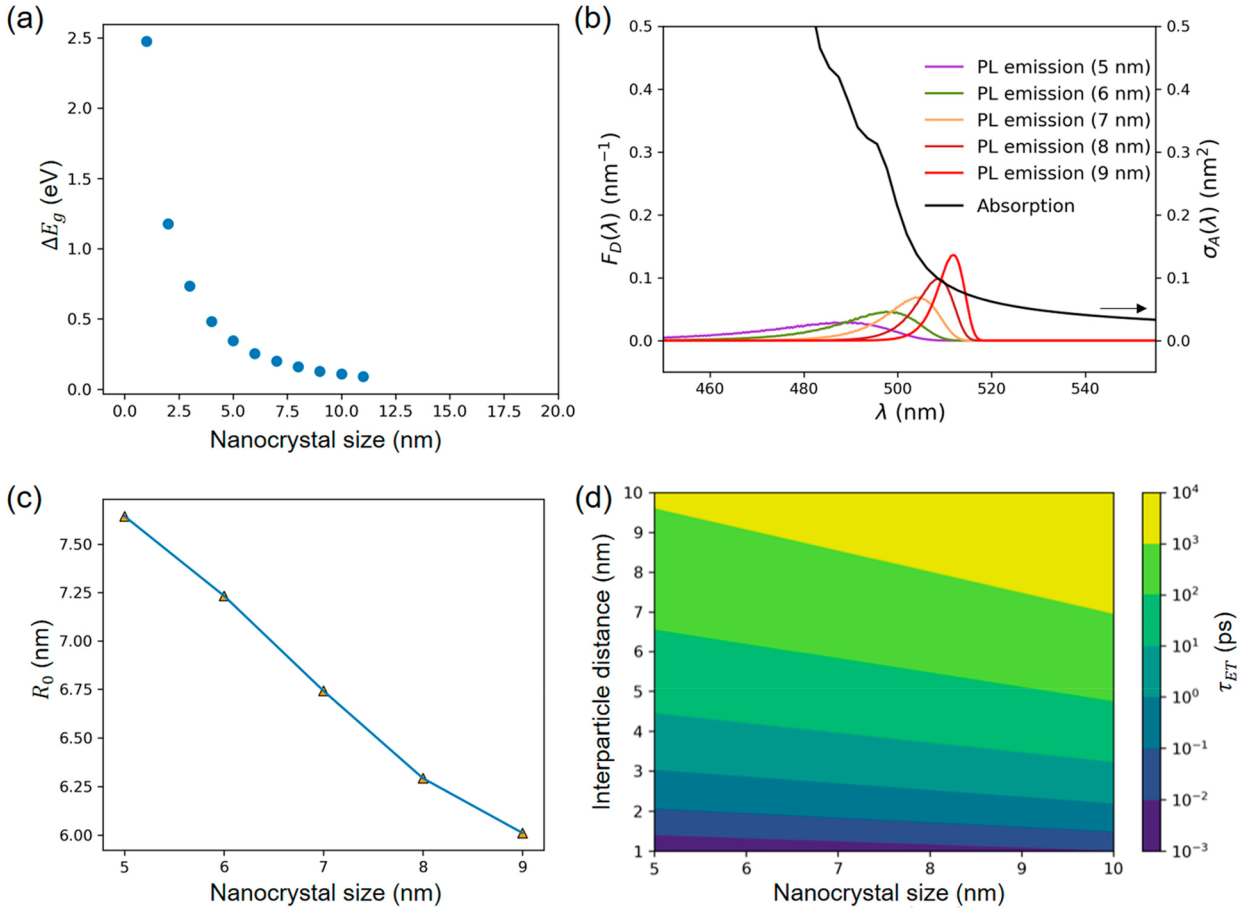

Figure 7. (a) Calculated band gap shift for $CsPbBr_3$ as a function of nanocrystal size. Solid blue circles are values obtained from solving a Schrödinger equation for an electron/hole and obtaining the band energy shifts. The calculations for $CsPbBr_3$ used effective carrier masses of $0.22m_e$ for the electron and $0.18m_e$ for the hole. (b) Calculated absorption cross-section $[\sigma_A(\lambda)]$ for 12 nm $CsPbBr_3$ acceptor and area-normalized PL spectra $[F_D(\lambda)]$ for nanocrystals of different sizes. (c) Calculated Förster radius, R_0, as a function of donor nanocrystal size. (d) Calculated FRET time (τ_{ET}, ps) as a function of interparticle distance (d, donor−acceptor separation) and donor nanocrystal size, plotted on a log scale with contour levels at every power of ten.

further comparison and unambiguous differentiation between the discussed phenomena.

In the absence of *in situ* characterization of superfluorescent domains, many of the optical properties attributable to cooperative emission could be explained by the loss of quantum confinement due to nanocrystal coalescence and formation of bulk-like particles, along with energy transfer and stimulated emission (lasing) that become efficient at cryogenic temperatures. The spectroscopic checks alone, such as steady-state reflectance or PL excitation measurements, which are sensitive to red-shifted absorption features, are insufficient to discern a collective lower-energy excitonic state from larger nanocrystals or bulk-like particles with smaller band gaps (Figure S7 and discussion above). In another study, an even faster superfluorescence (τ_{SF} = 4 ps at 77 K) was reported in $CsPbBr_3$ nanocrystal superlattices aged for 4−15 days at 10 °C under vacuum.[26] The TEM images of aged $CsPbBr_3$ nanocrystal superlattices in ref 26 show the presence of larger $CsPbBr_3$ particles among nanocrystals, similar to our observations (Figure 3b and Figure S9). That supports our case that aging has a significant effect on the optical properties of perovskite nanocrystal superlattices and should not be ignored nor confused with cooperative effects.

Evidence for Energy Transfer in Fresh and Aged Superlattices. The fresh and aged superlattices kept in vacuum present a compelling case for the investigation of energy transfer between $CsPbBr_3$ nanocrystals and bulk-like particles by means of transient spectrally resolved PL spectroscopy. Figure 6 reports cryogenic (T = 4 K) time-resolved PL spectra acquired from two individual superlattices from the same sample on day 0 (Figure 6a) and day 7 (Figure 6c) under low excitation fluence (10 and 25 μJ/cm^2, respectively). The spectrum of the fresh superlattice contained a single peak (consistent with steady-state measurements, Figure 1b), which underwent a transient shift of ≈9 meV to lower energy during the first ∼600 ps of the decay (Figure 6a, black dotted curve). Similarly, the double peak spectrum of the aged superlattice underwent a small ≈3 meV transient red shift of the lower-energy peak and a larger transient red shift (≈13 meV) of the higher-energy peak (Figure 6c, left and right black dotted curves, respectively). At low excitation fluence, such shifts point to the intra-superlattice energy transfer, paralleling the behavior of nanocrystal solids of metal chalcogenides.[44,46,47,89−91]

The characterization of the PL spectral dynamics was further elaborated by the energy-dependent PL intensity decays, plotted for both samples in Figure 6b,d. In the fresh

https://dx.doi.org/10.1021/acsnano.0c06595
ACS Nano 2021, 15, 650−664

superlattice (Figure 6b), the intensity decays at low PL energies were nearly monoexponential with a lifetime of $\tau_1 \approx$ 250 ps, a value similar to the reported radiative lifetimes of $CsPbBr_3$ nanocrystals at cryogenic temperatures.[1,4,55,62,92] As the PL energy increased, the decay of PL intensity became faster and multiexponential. The biexponential decays were fit with two lifetimes: τ_1 = 250 ps and τ_2 = 140 to 70 ps, with τ_2 becoming smaller as PL energy increases (Table S1). In the time-resolved PL spectrum of the aged superlattice (Figure 6c), two PL peaks were observed (consistent with the steady-state spectrum, Figure 2b): the intense low-energy one, stemming from the bulk-like $CsPbBr_3$ particles, and a much weaker high-energy peak, originating from the remaining $CsPbBr_3$ nanocrystals. The analysis of the energy-resolved PL decays (Figure 6d) revealed the single-exponential decay of the intense low-energy PL peak ($\tau_1' \approx$ 180−220 ps) and biexponential decay of the weak, high-energy PL peak (τ_1 = 250 ps; τ_2 = 130 to 50 ps; Table S2). In both cases (fresh and aged superlattices), the slower PL decay rates $k_1 = 1/\tau_1$ and $k_1' = 1/\tau_1'$ are interpreted as the average radiative exciton recombination rates, while the energy-dependent and faster rate $k_2 = 1/\tau_2$ is assigned to inter-nanocrystal energy transfer.[89,93]

To understand these spectral dynamics, we calculated the energy-transfer rates between differently sized $CsPbBr_3$ nanocrystals within the framework of Förster resonance electronic excitation transfer (FRET).[38,39] We consider an ensemble of FRET donors and acceptors in the superlattices as there is a distribution of nanocrystals of different sizes and, hence, different band gaps. Smaller nanocrystals with high-energy PL act as donors, whereas larger nanocrystals or bulk-like $CsPbBr_3$ particles act as acceptors. The FRET rate, k_{ET}, is inversely proportional to the 6th power of the donor−acceptor distance, d:

$$k_{ET} = \frac{1}{\tau_D}\left(\frac{R_0}{d}\right)^6 \quad (1)$$

where τ_D is the lifetime of the donor in the absence of an acceptor, set as the slow exponential component of the PL decay ($\tau_D = \tau_1$ = 250 ps).[38] R_0, the Förster radius, is a measure of the energy transfer efficiency. R_0 characterizes the distance where the energy-transfer process competes with other recombination processes such as radiative recombination decays.[94] R_0 depends on the spectral overlap between the acceptor and donor:

$$R_0^6 = \frac{9\eta_{PL}\kappa^2}{128\pi^5 n^4}\int \lambda^4 F_D(\lambda)\,\sigma_A(\lambda)\,d\lambda \quad (2)$$

where η_{PL} is the quantum yield assumed to be unity;[18,95] k is the orientation factor, equal to 2/3 for randomly oriented dipoles; n is the measured refractive index for $CsPbBr_3$ (1.93).[96] $F_D(\lambda)$ is the donor PL emission spectrum (area-normalized to 1) and $\sigma_A(\lambda)$ is the absorption cross-section of the acceptor.

Since the donors are smaller and acceptors are larger, we tuned the PL emission as a function of the nanocrystal size and fixed the absorption cross-section of bulk-like $CsPbBr_3$ to that of a 12 nm nanocrystal (the band gap changes marginally by ≈5 meV when increasing the nanocrystal size beyond 12 nm in Figure 7a, and the FRET rate does not vary significantly if the acceptor size changes, as illustrated in Figure S22 for 10 and 16 nm $CsPbBr_3$ nanocrystals). As the smaller $CsPbBr_3$ nanocrystals coalesce into bulk-like particles, the overall PL spectrum red shifts and sharpens, resulting in a decrease of the overlap with an absorption spectrum of the donor (Figure 7b). Therefore, the calculated R_0 decreases as nanocrystals grow (Figure 7c), changing from 7.6 to 6 nm when the donor size increases from 5 to 9 nm.

The energy-transfer rate and its corresponding lifetime, $\tau_{ET} = 1/k_{ET}$, can be estimated using eq 1. However, determining d, the effective donor−acceptor distance, needs to be scrutinized, since small changes in d will result in orders of magnitude differences in the final k_{ET} due to the $1/d^6$ scaling (eq 1). On one hand, a wall-to-wall distance of 2.2 nm between neighboring nanocrystals (estimated as the difference between ∼10.2 nm average superlattice periodicity in Figure 3a, and ∼8 nm average nanocrystal edge length) provides a lower bound for the d. On the other hand, the center-to-center distance between nanocrystals of ∼10 nm can be used as an upper bound for d. Therefore, we plot τ_{ET} as a function of both d and the nanocrystal size (Figure 7d) and observe that as the nanocrystal size or d increases, τ_{ET} increases rapidly, ranging from <1 to >1000 ps.

For any nanocrystal size in the range 5−10 nm and interparticle distance d < 4.5 nm, τ_{ET} is under 100 ps, which matches τ_2 extracted from the experimental data. In order to achieve faster energy transfer, smaller donor nanocrystals and shorter inter-nanocrystal separations are required. This trend matches the shortening of τ_2 from 140 to 50 ps with increasing PL energy (considering smaller nanocrystals as donors) for both fresh and aged $CsPbBr_3$ superlattices (Figure 6b,d, Tables S1 and S2). Thus, the calculated FRET rates suggest that the measured fast decay component τ_2 can be explained by interparticle energy transfer. This may allow for efficient exciton funneling into the acceptor sites (bulk-like $CsPbBr_3$ particles) and rationalizes their increased PL intensity in the aged superlattices. This prediction of ultrafast FRET explains the observation of sharp peaks from bulk-like $CsPbBr_3$ particles (acceptors) located on top of the superlattices (donor) aged in air by means of, *e.g.*, FRET-assisted lasing.[97,98] Despite the good agreement, large variations in the calculated τ_{ET} necessitate careful examination when using the FRET model. In addition to the uncertainty induced by estimating d, errors could propagate from experimentally determined values when recovering the prefactors in eq 2. Nevertheless, the FRET model helps to understand the qualitative trend of energy transfer using the nanocrystal size and separation as tuning knobs, which is useful in guiding future experiments.

CONCLUSIONS

The aging of self-assembled $CsPbBr_3$ nanocrystals in vacuum or in air is shown to produce optical signatures that mimic cooperative emission at cryogenic temperature: narrow, low-energy PL peaks with accelerated, oscillating emission decays. These optical features are related to bulk-like $CsPbBr_3$ particles and large nanocrystals forming in the superlattices. Despite the size uniformity and shape-pure qualities of the starting $CsPbBr_3$ nanocrystals, the labile cesium oleate ligands seem inadequate for the fabrication of long-lasting assemblies. On one hand, it is anticipated that further advances in the synthesis of surface-enhanced $CsPbX_3$ nanocrystals (such as ZnX_2-,[14,41] phosphonate-,[18,99,100] or zwitterion-capped[15,16] ones) or in optimized ligand exchanges (*e.g.*, with quaternary ammonium halides,[17] thiocyanates,[101] and other Lewis bases[102]) will enable the fabrication of assemblies that are

https://dx.doi.org/10.1021/acsnano.0c06595
ACS Nano 2021, 15, 650−664

resistant to aging and air exposure. A superlattice made from shape-pure $CsPbX_3$ nanocrystals with a near-unity photoluminescence quantum yield that are also stable against coalescence and reactivity in air is a desirable target for future studies and applications of collective phenomena. On the other hand, aging superlattices made from metastable $CsPbX_3$ nanocrystals is a way to produce nanomaterials with a heterogeneous energy landscape consisting of numerous donors and sparse acceptors. Such materials could be promising for investigations of energy transfer across several spatial and temporal length scales, as predicted by theoretical calculations. Ultrafast sub-picosecond energy transfer (already reported for lead halide perovskite quantum wells)[103] combined with the recent findings of extended exciton diffusion lengths in $CsPbBr_3$ nanocrystal solids[27,28,104,105] would make such energetically heterogeneous nanocrystal systems attractive candidates for light amplification and harvesting (*e.g.*, in artificial photosynthesis).

METHODS

Chemicals. Lead(II) acetate trihydrate (Sigma-Aldrich, ≥99.99% trace metal basis, cat. no. 467863), cesium carbonate (Sigma-Aldrich, Reagent Plus, 99%, cat. no. 441902), 1-octadecene (Sigma-Aldrich, technical grade, 90%, cat. no. O806), oleic acid (OA, Sigma-Aldrich, technical grade, 90%, cat. no. 364525), didodecylamine (DDAm, TCI, >97.0%, cat. no. D0267), benzoyl bromide (Sigma-Aldrich, 97%, cat. no. 139726), toluene (Sigma-Aldrich, anhydrous, cat. no. 244511), and ethyl acetate (EtOAc, Sigma-Aldrich, anhydrous, 99.8%, cat. no. 270989) were purchased as indicated. Benzoyl bromide was opened and handled inside a glovebox because it is an air- and moisture-sensitive compound; lead(II) acetate was weighted inside a glovebox and handled inside a ventilated fume hood because it is a lead poisoning hazard. All reagents were used as received.

Synthesis of $CsPbBr_3$ Nanocrystals. $CsPbBr_3$ nanocrystals were synthesized following the published procedure[31] with modifications. Modifications consisted of performing the synthesis in 40 mL vials in air and changes to nanocrystal purification (see below). The nanocrystal synthesis and self-assembly were carried out in five steps.

First Step: Stock Solution of Cesium and Lead Oleates [(Cs, Pb)-oleates]. A 760 mg amount of lead(II) acetate trihydrate, 160 mg of cesium carbonate, and 13.4 g of OA were combined in a 40 mL vial equipped with a magnetic stirring bar and a thermocouple. The mixture was heated to 120−130 °C for 3 h under a continuous flow of nitrogen, forming a clear, light-yellow solution.

Second Step: Reaction Setup. A different 40 mL glass vial was equipped with a magnetic stirrer and a thermocouple, and 443 mg of DDAm was combined in it with 10 mL of ODE and 1.5 mL of (Cs, Pb)-oleates stock solution. The vial was heated to ∼110−130 °C on the hot plate and kept at that temperature for ∼5 min, producing a clear homogeneous mixture. After 5 min had passed, the vial was removed from the hot plate and suspended in the air above a magnetic stirring plate to cool under vigorous stirring.

Third Step: $CsPbBr_3$ Nanocrystal Nucleation and Growth. In the glovebox, 60 μL (∼101 ± 3 mg) of benzoyl bromide (measured with a 100 μL mechanical pipet) was combined with 0.6 mL of ODE in a 4 mL vial, mixed by manual shaking and filled into a 1 mL disposable plastic syringe equipped with an 18G needle. The syringe was taken outside of the glovebox, and the benzoyl bromide−ODE solution was injected into the mixture of (Cs,Pb)-oleates/DDAm/ODE at 80−85 °C. The reaction mixture turned bright green-yellow immediately after the injection. The reaction mixture was allowed to cool while stirring.

Fourth Step, NC Isolation. Once the reaction cooled to room temperature (21−23 °C), a 1−1.5 mL aliquot of the crude reaction mixture was filtered through a 0.45 μm PTFE syringe filter into an 8 mL vial and anhydrous EtOAc gradually added to it in small portions under gentle manual shaking. Once the mixture started to turn cloudy (at ∼3−4 mL of added EtOAc), the addition of EtOAc was stopped and the vial was centrifuged at 5000 rpm for 3 min. The centrifugation resulted in the accumulation of bright green precipitate of $CsPbBr_3$ nanocrystals on one side of the vial, covered by a clear supernatant. The supernatant was discarded, and the residual nanocrystal solid was centrifuged again at 5000 rpm for 1 min to collect any residual liquid, which was subsequently removed using a cotton tip. The remaining bright green solid of $CsPbBr_3$ nanocrystals was dried under a flow of nitrogen for 5−10 min.

Fifth Step, $CsPbBr_3$ Nanocrystal Self-Assembly (Fresh Superlattices). After the bright green solid of nanocrystals finished drying under nitrogen flow, it was dispersed in ∼400−500 μL of anhydrous toluene. Shortly after, a 10−30 μL drop of the nanocrystal dispersion was deposited onto the polished side of the Si wafer (Ted Pella, ∼0.5 mm thick, cat. no. 16006, cut to 10 × 10 mm^2 or 5 × 5 mm^2 depending on the experiment) and the toluene was allowed to evaporate under a flow of nitrogen or an ambient atmosphere inside the fume hood. The solvent evaporation time was typically ∼5−20 min, depending on the exact conditions. After the toluene evaporated (by visual inspection), the Si wafer with nanocrystals was placed under a low vacuum (0.4−0.7 mbar) for ∼10−20 min to remove any residual trapped solvent. After that step, the sample was inspected under an optical microscope for the presence of superlattices. The deposition conditions such as concentration and volumes of the deposited dispersion were varied to produce Si wafers with areas of isolated rectangular-shaped superlattices. Prior to the cryogenic experiments, it is suggested to inspect the superlattice samples with micro-PL at room temperature to ensure the absence of bulk-like impurities on their surface. The bulk-like impurities would appear as bright spots, and if they are detected, it is likely that $CsPbBr_3$ nanocrystals have started to react with the atmosphere and the resulting products will obscure the optical response of the pristine nanocrystal superlattice.

Aging of Superlattices. The aging of superlattices under vacuum at room temperature was accomplished either by storing the samples under medium vacuum (0.4−0.7 mbar) in a plate degasser (Edwards Vacuum, PD3) or leaving them in the cryostat, or by vacuum-sealing them in a secondary container inside a nitrogen-filled glovebox with the help of a commercial device (Laica VT31200). The superlattice aging occurred in a similar way regardless of the vacuuming method, as long as there was no continuous air exposure. The aging of $CsPbBr_3$ nanocrystals in dispersion or superlattices in the air was accomplished by leaving the sample under the ambient atmosphere in the laboratory for a few days (typical conditions are T = 21−23 °C and variable relative humidity of 50−75%). Superlattices showed the first signs of large particle formation overnight (the ∼10−20 min vacuum exposure after self-assembly slows the formation of large particles). The appearance of cloudiness and small amounts of white-yellow precipitate were the first signs of nanocrystal reactivity with air in dispersion.

Structural and Optical Characterization. The steady-state optical absorbance and PL spectra of $CsPbBr_3$ nanocrystals in dilute toluene dispersion were recorded with Cary 500 UV−vis spectrophotometer and Cary Eclipse spectrofluorimeter (λ_{exc} = 350 or 400 nm). X-ray diffraction analyses of the superlattice aging and products of $CsPbBr_3$ nanocrystal air exposure were performed using a PANalytical Empyrean diffractometer equipped with a Cu Kα cathode (λ = 1.5406 Å), operating at 45 kV voltage and 50 mA current. Transmission electron microscopy (TEM) characterization of as-synthesized and aged $CsPbBr_3$ nanocrystals and dissolved superlattices was performed using a JEOL JEM 1400-Plus microscope operating at 120 kV accelerating voltage. The samples for TEM were prepared by drop-casting sample dispersion in toluene on top of a carbon-coated copper grid. Scanning electron microscopy (SEM) and elemental analysis by means of energy-dispersive X-ray spectroscopy characterization of the samples was performed using either a JEOL JSM-6490LA (low-resolution) or JSM-7500FA (high-resolution) microscope. For the imaging of the aged superlattices in cross-section, the Si wafer carrying aged superlattices on top was gently broken in two halves. Prior to breaking, the back of the wafer (the side without a superlattice) was scored with a diamond scribe pen.

https://dx.doi.org/10.1021/acsnano.0c06595
ACS Nano 2021, 15, 650−664

Room-temperature micro-PL images and spectra were collected using Nikon A1 laser scanning confocal microscope with 400 nm CW excitation, as described in the prior work.[48] For the micro-PL experiments at cryogenic temperatures, the sample was cooled in a closed-loop helium cryostat (Attocube) equipped with a 50× microscope objective (N.A. = 0.82) and working in a reflection configuration. In the steady-state micro-PL experiments, the $CsPbBr_3$ nanocrystal superlattices were excited with a continuous-wave excitation λ = 488 nm (Spectra-Physics). Broadband output of a xenon lamp light source (Korea Spectral Products-ASB-XE-175) was used for reflectivity measurements. The signal from the sample was projected on the entrance slits of a spectrometer (Horiba Jobin Yvon, iHR550) and coupled to a CCD camera (Hamamatsu, C9100 EM-CCD), which allows collecting either real space reflectivity/PL maps or energy-resolved maps. The fwhm of the excitation spot in real space was adjusted to match the lateral dimension of the superlattices (fwhm ≈ lateral size). In some cases, when measuring the PL spectra close to the excitation wavelength, a long-pass filter (Thorlabs FEL0500) was used to remove the residual signal of the excitation laser. The filtering effect of the long-pass filter onto the PL spectrum of the superlattices was either minimal or accounted for by correcting the experimental spectrum with a long-pass filter transmission during the data processing. For the time-resolved PL measurements, the samples were excited with a pulsed ∼50 fs laser at 10 kHz repetition rate and (λ_{exc} = 470 nm (Coherent, Topas Prime). The detected signal was focused on the same spectrometer coupled to a streak camera (Hamamatsu C10910 equipped with a C9300 CCD) with an overall temporal resolution of ∼1.5 ps.

A Michelson interferometer, equipped with a retroreflector and a motorized delay line along with one of the two arms, was used for first-order spatial and temporal coherence measurements.[106,107] The two emission bands of the aged superlattices were spectrally separated by using a notch filter (fwhm = 50 meV), and the fringe visibility [$v = (I_{max} - I_{min})/(I_{max} + I_{min})$] was evaluated from the multiple real space micro-PL images collected by scanning the time delay between the two arms. A Gaussian function was used to fit the fringe visibility decay, and the coherence time is extracted at $1/e^2$ intensity decay of the Gaussian fit. In order to measure the second-order correlation $g^{(2)}(\tau)$ function, the samples were excited with a pulsed ∼100 fs laser at 80 MHz repetition rate and λ_{exc} = 405 nm. The emitted PL was sent into a monochromator, spectrally filtered (∼0.2 nm) and then measured by a time correlated single photon counting module in the standard Hanbury Brown−Twiss configuration.

Theoretical Calculations. For a finite potential well, the tunneling probability can be calculated using a simple particle-in-a-box model. The wave function of an electron/hole is confined in a one-dimensional well that is 8 nm long and 3.85 eV deep, which are the size and the work function of a model $CsPbBr_3$ nanocrystal, respectively. The wave function is of the form $\Psi = Ae^{-\beta x}$, where $\beta = \sqrt{\frac{2m(U_0 - E_k)}{\hbar^2}}$. The wave function decays rapidly outside the potential well, with the tail of the work function being the main limiting factor for the wave function leakage (Figure S4).[66] The effective width of the ground-state wave function of an electron is calculated to be 8.39 nm, penetrating 0.39 nm outside the quantum well.

The absorption spectrum is calculated from the imaginary part of the dielectric function of $CsPbBr_3$ using the QUANTUM ESPRESSO density functional theory software suite.[108,109] The PBE functional was used with a 90 Ry energy cutoff and 18 × 18 × 18 Monkhorst−Pack k-point mesh for the cubic primitive cell.[110−112] To correct for the quasi-particle self-energy, we used the scissor correction of 1.02 eV to match the GW band gap when calculating the dielectric constant:

$$\epsilon_2(\omega) = \epsilon_2^{DFT}(\omega - \Delta/\hbar)$$

where Δ = 1.02 eV. It has been shown that it is sufficient to shift the DFT $\epsilon(\omega)$ by $\Delta/\hbar$ along the frequency axis to get the correct optical spectrum within the GW scissors-operator approximation.[113] The bulk absorption spectrum was shifted by another 5 meV to match the 12 nm nanocrystal band gap shift from quantum confinement effects. Gaussian smearing of 0.05 eV was used to obtain a smooth spectrum. The absorption cross-section was obtained using the following equation: $\sigma(\omega) = \epsilon(\omega)V\omega/(cn)$, where V is the volume of a 12 nm cubic nanocrystal, c is the speed of light, and n is the refractive index (1.93).

ASSOCIATED CONTENT

Supporting Information

The Supporting Information is available free of charge at https://pubs.acs.org/doi/10.1021/acsnano.0c06595.

Optical absorption and PL spectra, TEM and SEM images of nanocrystals, fresh and aged superlattices; room temperature and cryogenic micro-PL images, spectra, and decays for fresh and aged superlattices; cryogenic reflectance spectra of fresh and aged superlattices and first- and second-order coherence measurements; XRD patterns of superlattice aging; characterization of products due to the aging of $CsPbBr_3$ nanocrystals in air; time- and spectrally-resolved PL decays, PL fluence-dependence, and optical gain spectra of the products of aging; tables of energy-resolved PL decay fit parameters; calculated wavefunction, size distributions and ensemble PL spectra, R_0 and FRET rates (PDF)

AUTHOR INFORMATION

Corresponding Authors

Dmitry Baranov − *Nanochemistry Department, Italian Institute of Technology, Genova 16163, Italy;* orcid.org/0000-0001-6439-8132; Email: dmitry.baranov@iit.it

Liang Z. Tan − *Molecular Foundry, Lawrence Berkeley National Laboratory, Berkeley, California 94720, United States;* orcid.org/0000-0003-4724-6369; Email: lztan@lbl.gov

Daniele Sanvitto − *CNR Nanotec, Institute of Nanotechnology, Lecce 73100, Italy;* Email: daniele.sanvitto@nanotec.cnr.it

Liberato Manna − *Nanochemistry Department, Italian Institute of Technology, Genova 16163, Italy;* orcid.org/0000-0003-4386-7985; Email: liberato.manna@iit.it

Authors

Antonio Fieramosca − *CNR Nanotec, Institute of Nanotechnology, Lecce 73100, Italy*

Ruo Xi Yang − *Molecular Foundry, Lawrence Berkeley National Laboratory, Berkeley, California 94720, United States*

Laura Polimeno − *CNR Nanotec, Institute of Nanotechnology, Lecce 73100, Italy; Dipartimento di Matematica e Fisica "E. de Giorgi", Università Del Salento, Lecce 73100, Italy*

Giovanni Lerario − *CNR Nanotec, Institute of Nanotechnology, Lecce 73100, Italy*

Stefano Toso − *Nanochemistry Department, Italian Institute of Technology, Genova 16163, Italy; International Doctoral Program in Science, Università Cattolica del Sacro Cuore, Brescia 25121, Italy*

Carlo Giansante − *CNR Nanotec, Institute of Nanotechnology, Lecce 73100, Italy;* orcid.org/0000-0003-4558-5367

https://dx.doi.org/10.1021/acsnano.0c06595
ACS Nano 2021, 15, 650−664

Milena De Giorgi − *CNR Nanotec, Institute of Nanotechnology, Lecce 73100, Italy;* orcid.org/0000-0002-4522-7933

Complete contact information is available at: https://pubs.acs.org/10.1021/acsnano.0c06595

Author Contributions

D.B., L.M., and D.S. conceived the project. D.B. synthesized the samples; A.F., L.P., G.L., M.D.G., and D.B. performed optical experiments; D.B. and S.T. performed structural characterization of superlattices. R.X.Y. and L.Z.T. performed computational modeling of electronic structure and energy transfer. D.B. drafted the manuscript with contributions from all coauthors.

Notes

The authors declare no competing financial interest.

ACKNOWLEDGMENTS

The work of D.B. was supported by the European Union's Horizon 2020 research and innovation program under the Marie Sklodowska-Curie Grant Agreement No. 794560 (RETAIN). R.X.Y. and L.Z.T. were supported by the Molecular Foundry, a DOE Office of Science User Facility of the Office of Science of the U.S. Department of Energy under Contract No. DE-AC02-05CH11231. D.S. acknowledges support from the project PRIN Interacting Photons in Polariton Circuits—INPhoPOL (Ministry of University and Scientific Research, MIUR, 2017P9FJBS_001). We thank P. Cazzato, L. De Marco, D. Ballarini, D. G. Suárez-Forero, V. Ardizzone, L. Dominici, L. Carbone (CNR Nanotec), and G. La Rosa (IIT) for helpful discussions and technical assistance, and S. Lauciello (Electron Microscopy Facility at IIT) for help with HRSEM analysis of fresh and aged superlattices.

REFERENCES

(1) Becker, M. A.; Vaxenburg, R.; Nedelcu, G.; Sercel, P. C.; Shabaev, A.; Mehl, M. J.; Michopoulos, J. G.; Lambrakos, S. G.; Bernstein, N.; Lyons, J. L.; Stöferle, T.; Mahrt, R. F.; Kovalenko, M. V.; Norris, D. J.; Rainò, G.; Efros, A. L. Bright Triplet Excitons in Caesium Lead Halide Perovskites. *Nature* **2018**, *553*, 189−193.

(2) Sercel, P. C.; Lyons, J. L.; Wickramaratne, D.; Vaxenburg, R.; Bernstein, N.; Efros, A. L. Exciton Fine Structure in Perovskite Nanocrystals. *Nano Lett.* **2019**, *19*, 4068−4077.

(3) Sercel, P. C.; Lyons, J. L.; Bernstein, N.; Efros, A. L. Quasicubic Model for Metal Halide Perovskite Nanocrystals. *J. Chem. Phys.* **2019**, *151*, 234106.

(4) Rainò, G.; Nedelcu, G.; Protesescu, L.; Bodnarchuk, M. I.; Kovalenko, M. V.; Mahrt, R. F.; Stöferle, T. Single Cesium Lead Halide Perovskite Nanocrystals at Low Temperature: Fast Single-Photon Emission, Reduced Blinking, and Exciton Fine Structure. *ACS Nano* **2016**, *10*, 2485−2490.

(5) Li, B.; Huang, H.; Zhang, G.; Yang, C.; Guo, W.; Chen, R.; Qin, C.; Gao, Y.; Biju, V. P.; Rogach, A. L.; Xiao, L.; Jia, S. Excitons and Biexciton Dynamics in Single $CsPbBr_3$ Perovskite Quantum Dots. *J. Phys. Chem. Lett.* **2018**, *9*, 6934−6940.

(6) Becker, M. A.; Scarpelli, L.; Nedelcu, G.; Rainò, G.; Masia, F.; Borri, P.; Stöferle, T.; Kovalenko, M. V.; Langbein, W.; Mahrt, R. F. Long Exciton Dephasing Time and Coherent Phonon Coupling in $CsPbBr_2Cl$ Perovskite Nanocrystals. *Nano Lett.* **2018**, *18*, 7546−7551.

(7) Hu, F.; Zhang, H.; Sun, C.; Yin, C.; Lv, B.; Zhang, C.; Yu, W. W.; Wang, X.; Zhang, Y.; Xiao, M. Superior Optical Properties of Perovskite Nanocrystals As Single Photon Emitters. *ACS Nano* **2015**, *9*, 12410−12416.

(8) Fu, M.; Tamarat, P.; Trebbia, J.-B.; Bodnarchuk, M. I.; Kovalenko, M. V.; Even, J.; Lounis, B. Unraveling Exciton-Phonon Coupling in Individual $FAPbI_3$ Nanocrystals Emitting Near-Infrared Single Photons. *Nat. Commun.* **2018**, *9*, 3318.

(9) Utzat, H.; Sun, W.; Kaplan, A. E. K.; Krieg, F.; Ginterseder, M.; Spokoyny, B.; Klein, N. D.; Shulenberger, K. E.; Perkinson, C. F.; Kovalenko, M. V.; Bawendi, M. G. Coherent Single-Photon Emission from Colloidal Lead Halide Perovskite Quantum Dots. *Science* **2019**, *363*, 1068−1072.

(10) Pierini, S.; D'Amato, M.; Goyal, M.; Glorieux, Q.; Giacobino, E.; Lhuillier, E.; Couteau, C.; Bramati, A. Highly Photo-Stable Perovskite Nanocubes: Towards Integrated Single Photon Sources Based on Tapered Nanofibers. *ACS Photonics* **2020**, *7*, 2265−2272.

(11) Bodnarchuk, M. I.; Boehme, S. C.; Ten Brinck, S.; Bernasconi, C.; Shynkarenko, Y.; Krieg, F.; Widmer, R.; Aeschlimann, B.; Günther, D.; Kovalenko, M. V.; Infante, I. Rationalizing and Controlling the Surface Structure and Electronic Passivation of Cesium Lead Halide Nanocrystals. *ACS Energy Lett.* **2019**, *4*, 63−74.

(12) Quarta, D.; Imran, M.; Capodilupo, A.-L.; Petralanda, U.; van Beek, B.; De Angelis, F.; Manna, L.; Infante, I.; De Trizio, L.; Giansante, C. Stable Ligand Coordination at the Surface of Colloidal $CsPbBr_3$ Nanocrystals. *J. Phys. Chem. Lett.* **2019**, *10*, 3715−3726.

(13) Almeida, G.; Infante, I.; Manna, L. Resurfacing Halide Perovskite Nanocrystals. *Science* **2019**, *364*, 833−834.

(14) Woo, J. Y.; Kim, Y.; Bae, J.; Kim, T. G.; Kim, J. W.; Lee, D. C.; Jeong, S. Highly Stable Cesium Lead Halide Perovskite Nanocrystals through *in Situ* Lead Halide Inorganic Passivation. *Chem. Mater.* **2017**, *29*, 7088−7092.

(15) Krieg, F.; Ochsenbein, S. T.; Yakunin, S.; Ten Brinck, S.; Aellen, P.; Süess, A.; Clerc, B.; Guggisberg, D.; Nazarenko, O.; Shynkarenko, Y.; Kumar, S.; Shih, C.-J.; Infante, I.; Kovalenko, M. V. Colloidal $CsPbX_3$ (X = Cl, Br, I) Nanocrystals 2.0: Zwitterionic Capping Ligands for Improved Durability and Stability. *ACS Energy Lett.* **2018**, *3*, 641−646.

(16) Krieg, F.; Ong, Q. K.; Burian, M.; Rainò, G.; Naumenko, D.; Amenitsch, H.; Suess, A.; Grotevent, M. J.; Krumeich, F.; Bodnarchuk, M. I.; Shorubalko, I.; Stellacci, F.; Kovalenko, M. V. Stable Ultraconcentrated and Ultradilute Colloids of $CsPbX_3$ (X = Cl, Br) Nanocrystals Using Natural Lecithin as a Capping Ligand. *J. Am. Chem. Soc.* **2019**, *141*, 19839−19849.

(17) Imran, M.; Ijaz, P.; Goldoni, L.; Maggioni, D.; Petralanda, U.; Prato, M.; Almeida, G.; Infante, I.; Manna, L. Simultaneous Cationic and Anionic Ligand Exchange For Colloidally Stable $CsPbBr_3$ Nanocrystals. *ACS Energy Lett.* **2019**, *4*, 819−824.

(18) Zhang, B.; Goldoni, L.; Zito, J.; Dang, Z.; Almeida, G.; Zaccaria, F.; de Wit, J.; Infante, I.; De Trizio, L.; Manna, L. Alkyl Phosphonic Acids Deliver $CsPbBr_3$ Nanocrystals with High Photoluminescence Quantum Yield and Truncated Octahedron Shape. *Chem. Mater.* **2019**, *31*, 9140−9147.

(19) Collier, C. P.; Vossmeyer, T.; Heath, J. R. Nanocrystal Superlattices. *Annu. Rev. Phys. Chem.* **1998**, *49*, 371−404.

(20) Murray, C. B.; Kagan, C. R.; Bawendi, M. G. Synthesis and Characterization of Monodisperse Nanocrystals and Close-Packed Nanocrystal Assemblies. *Annu. Rev. Mater. Sci.* **2000**, *30*, 545−610.

(21) Boles, M. A.; Engel, M.; Talapin, D. V. Self-Assembly of Colloidal Nanocrystals: From Intricate Structures to Functional Materials. *Chem. Rev.* **2016**, *116*, 11220−11289.

(22) Jurow, M. J.; Lampe, T.; Penzo, E.; Kang, J.; Koc, M. A.; Zechel, T.; Nett, Z.; Brady, M.; Wang, L.-W.; Alivisatos, A. P.; Cabrini, S.; Brütting, W.; Liu, Y. Tunable Anisotropic Photon Emission from Self-Organized $CsPbBr_3$ Perovskite Nanocrystals. *Nano Lett.* **2017**, *17*, 4534−4540.

(23) Tong, Y.; Yao, E.-P.; Manzi, A.; Bladt, E.; Wang, K.; Döblinger, M.; Bals, S.; Müller-Buschbaum, P.; Urban, A. S.; Polavarapu, L.; Feldmann, J. Spontaneous Self-Assembly of Perovskite Nanocrystals into Electronically Coupled Supercrystals: Toward Filling the Green Gap. *Adv. Mater.* **2018**, *30*, 1801117.

(24) van der Burgt, J. S.; Geuchies, J. J.; van der Meer, B.; Vanrompay, H.; Zanaga, D.; Zhang, Y.; Albrecht, W.; Petukhov, A. V.; Filion, L.; Bals, S.; Swart, I.; Vanmaekelbergh, D. Cuboidal

Supraparticles Self-Assembled from Cubic $CsPbBr_3$ Perovskite Nanocrystals. *J. Phys. Chem. C* **2018**, *122*, 15706−15712.
(25) Rainò, G.; Becker, M. A.; Bodnarchuk, M. I.; Mahrt, R. F.; Kovalenko, M. V.; Stöferle, T. Superfluorescence from Lead Halide Perovskite Quantum Dot Superlattices. *Nature* **2018**, *563*, 671−675.
(26) Zhou, C.; Zhong, Y.; Dong, H.; Zheng, W.; Tan, J.; Jie, Q.; Pan, A.; Zhang, L.; Xie, W. Cooperative Excitonic Quantum Ensemble in Perovskite-Assembly Superlattice Microcavities. *Nat. Commun.* **2020**, *11*, 329.
(27) Yang, M.; Moroz, P.; Miller, E.; Porotnikov, D.; Cassidy, J.; Ellison, C.; Medvedeva, X.; Klinkova, A.; Zamkov, M. Energy Transport in $CsPbBr_3$ Perovskite Nanocrystal Solids. *ACS Photonics* **2020**, *7*, 154−164.
(28) Penzo, E.; Loiudice, A.; Barnard, E. S.; Borys, N. J.; Jurow, M. J.; Lorenzon, M.; Rajzbaum, I.; Wong, E. K.; Liu, Y.; Schwartzberg, A. M.; Cabrini, S.; Whitelam, S.; Buonsanti, R.; Weber-Bargioni, A. Long-Range Exciton Diffusion in Two-Dimensional Assemblies of Cesium Lead Bromide Perovskite Nanocrystals. *ACS Nano* **2020**, *14*, 6999−7007.
(29) Vila-Liarte, D.; Feil, M. W.; Manzi, A.; Garcia-Pomar, J. L.; Huang, H.; Döblinger, M.; Liz-Marzán, L. M.; Feldmann, J.; Polavarapu, L.; Mihi, A. Templated-Assembly of $CsPbBr_3$ Perovskite Nanocrystals into 2D Photonic Supercrystals with Amplified Spontaneous Emission. *Angew. Chem., Int. Ed.* **2020**, *59*, 17750−17756.
(30) Huang, H.; Feil, M. W.; Fuchs, S.; Debnath, T.; Richter, A. F.; Tong, Y.; Wu, L.; Wang, Y.; Döblinger, M.; Nickel, B. Growth of Perovskite $CsPbBr_3$ Nanocrystals and Their Formed Superstructures Revealed by *in Situ* Spectroscopy. *Chem. Mater.* **2020**, *32*, 8877−8884.
(31) Imran, M.; Ijaz, P.; Baranov, D.; Goldoni, L.; Petralanda, U.; Akkerman, Q.; Abdelhady, A. L.; Prato, M.; Bianchini, P.; Infante, I.; Manna, L. Shape-Pure, Nearly Monodispersed $CsPbBr_3$ Nanocubes Prepared Using Secondary Aliphatic Amines. *Nano Lett.* **2018**, *18*, 7822−7831.
(32) Imran, M.; Caligiuri, V.; Wang, M.; Goldoni, L.; Prato, M.; Krahne, R.; De Trizio, L.; Manna, L. Benzoyl Halides as Alternative Precursors for the Colloidal Synthesis of Lead-Based Halide Perovskite Nanocrystals. *J. Am. Chem. Soc.* **2018**, *140*, 2656−2664.
(33) Nagaoka, Y.; Hills-Kimball, K.; Tan, R.; Li, R.; Wang, Z.; Chen, O. Nanocube Superlattices of Cesium Lead Bromide Perovskites and Pressure-Induced Phase Transformations at Atomic and Mesoscale Levels. *Adv. Mater.* **2017**, *29*, 1606666.
(34) Zhang, Y.; Thomas, C. J.; Guillaussier, A.; Smilgies, D.-M.; Korgel, B. A. Thermal Phase Transitions in Superlattice Assemblies of Cuboidal $CH_3NH_3PbI_3$ Nanocrystals Followed by Grazing Incidence X-Ray Scattering. *J. Phys. Chem. C* **2019**, *123*, 17555−17565.
(35) Zhang, Y.; Shah, T.; Deepak, F. L.; Korgel, B. A. Surface Science and Colloidal Stability of Double-Perovskite $Cs_2AgBiBr_6$ Nanocrystals and Their Superlattices. *Chem. Mater.* **2019**, *31*, 7962−7969.
(36) Thomas, C. J.; Zhang, Y.; Guillaussier, A.; Bdeir, K.; Aly, O. F.; Kim, H. G.; Noh, J.; Reimnitz, L. C.; Li, J.; Deepak, F. L.; Smilgies, D.-M.; Milliron, D. J.; Korgel, B. A. Thermal Stability of the Black Perovskite Phase in Cesium Lead Iodide Nanocrystals under Humid Conditions. *Chem. Mater.* **2019**, *31*, 9750−9758.
(37) Brennan, M. C.; Toso, S.; Pavlovetc, I. M.; Zhukovskyi, M.; Marras, S.; Kuno, M.; Manna, L.; Baranov, D. Superlattices Are Greener on the Other Side: How Light Transforms Self-Assembled Mixed Halide Perovskite Nanocrystals. *ACS Energy Lett.* **2020**, *5*, 1465−1473.
(38) Allan, G.; Delerue, C. Energy Transfer between Semiconductor Nanocrystals: Validity of Förster's Theory. *Phys. Rev. B: Condens. Matter Mater. Phys.* **2007**, *75*, 195311.
(39) Curutchet, C.; Franceschetti, A.; Zunger, A.; Scholes, G. D. Examining Förster Energy Transfer for Semiconductor Nanocrystalline Quantum Dot Donors and Acceptors. *J. Phys. Chem. C* **2008**, *112*, 13336−13341.
(40) Utzat, H.; Shulenberger, K. E.; Achorn, O. B.; Nasilowski, M.; Sinclair, T. S.; Bawendi, M. G. Probing Linewidths and Biexciton Quantum Yields of Single Cesium Lead Halide Nanocrystals in Solution. *Nano Lett.* **2017**, *17*, 6838−6846.
(41) Dong, Y.; Qiao, T.; Kim, D.; Parobek, D.; Rossi, D.; Son, D. H. Precise Control of Quantum Confinement in Cesium Lead Halide Perovskite Quantum Dots *via* Thermodynamic Equilibrium. *Nano Lett.* **2018**, *18*, 3716−3722.
(42) Brennan, M. C.; Herr, J. E.; Nguyen-Beck, T. S.; Zinna, J.; Draguta, S.; Rouvimov, S.; Parkhill, J.; Kuno, M. Origin of the Size-Dependent Stokes Shift in $CsPbBr_3$ Perovskite Nanocrystals. *J. Am. Chem. Soc.* **2017**, *139*, 12201−12208.
(43) Leatherdale, C. A.; Bawendi, M. G. Observation of Solvatochromism in CdSe Colloidal Quantum Dots. *Phys. Rev. B: Condens. Matter Mater. Phys.* **2001**, *63*, 165315.
(44) Wuister, S. F.; Koole, R.; de Mello Donegá, C.; Meijerink, A. Temperature-Dependent Energy Transfer in Cadmium Telluride Quantum Dot Solids. *J. Phys. Chem. B* **2005**, *109*, 5504−5508.
(45) Wolcott, A.; Doyeux, V.; Nelson, C. A.; Gearba, R.; Lei, K. W.; Yager, K. G.; Dolocan, A. D.; Williams, K.; Nguyen, D.; Zhu, X. Y. Anomalously Large Polarization Effect Responsible for Excitonic Red Shifts in PbSe Quantum Dot Solids. *J. Phys. Chem. Lett.* **2011**, *2*, 795−800.
(46) Kagan, C. R.; Murray, C. B.; Bawendi, M. G. Long-Range Resonance Transfer of Electronic Excitations in Close-Packed CdSe Quantum-Dot Solids. *Phys. Rev. B: Condens. Matter Mater. Phys.* **1996**, *54*, 8633−8643.
(47) Kagan, C. R.; Murray, C. B.; Nirmal, M.; Bawendi, M. G. Electronic Energy Transfer in CdSe Quantum Dot Solids. *Phys. Rev. Lett.* **1996**, *76*, 1517−1520.
(48) Baranov, D.; Toso, S.; Imran, M.; Manna, L. Investigation into the Photoluminescence Red Shift in Cesium Lead Bromide Nanocrystal Superlattices. *J. Phys. Chem. Lett.* **2019**, *10*, 655−660.
(49) Guyot-Sionnest, P. Electrical Transport in Colloidal Quantum Dot Films. *J. Phys. Chem. Lett.* **2012**, *3*, 1169−1175.
(50) Kagan, C. R.; Murray, C. B. Charge Transport in Strongly Coupled Quantum Dot Solids. *Nat. Nanotechnol.* **2015**, *10*, 1013.
(51) Lee, J.-S.; Kovalenko, M. V.; Huang, J.; Chung, D. S.; Talapin, D. V. Band-Like Transport, High Electron Mobility and High Photoconductivity in All-Inorganic Nanocrystal Arrays. *Nat. Nanotechnol.* **2011**, *6*, 348−352.
(52) Whitham, K.; Yang, J.; Savitzky, B. H.; Kourkoutis, L. F.; Wise, F.; Hanrath, T. Charge Transport and Localization in Atomically Coherent Quantum Dot Solids. *Nat. Mater.* **2016**, *15*, 557−563.
(53) Wright, A. D.; Verdi, C.; Milot, R. L.; Eperon, G. E.; Pérez-Osorio, M. A.; Snaith, H. J.; Giustino, F.; Johnston, M. B.; Herz, L. M. Electron-Phonon Coupling in Hybrid Lead Halide Perovskites. *Nat. Commun.* **2016**, *7*, 11755.
(54) Iaru, C. M.; Geuchies, J. J.; Koenraad, P. M.; Vanmaekelbergh, D.; Silov, A. Y. Strong Carrier-Phonon Coupling in Lead Halide Perovskite Nanocrystals. *ACS Nano* **2017**, *11*, 11024−11030.
(55) Diroll, B. T.; Zhou, H.; Schaller, R. D. Low-Temperature Absorption, Photoluminescence, and Lifetime of $CsPbX_3$ (X = Cl, Br, I) Nanocrystals. *Adv. Funct. Mater.* **2018**, *28*, 1800945.
(56) Ramade, J.; Andriambariarijaona, L. M.; Steinmetz, V.; Goubet, N.; Legrand, L.; Barisien, T.; Bernardot, F.; Testelin, C.; Lhuillier, E.; Bramati, A.; Chamarro, M. Exciton-Phonon Coupling in a $CsPbBr_3$ Single Nanocrystal. *Appl. Phys. Lett.* **2018**, *112*, 072104.
(57) Guo, Y.; Yaffe, O.; Hull, T. D.; Owen, J. S.; Reichman, D. R.; Brus, L. E. Dynamic Emission Stokes Shift and Liquid-Like Dielectric Solvation of Band Edge Carriers in Lead-Halide Perovskites. *Nat. Commun.* **2019**, *10*, 1175.
(58) Toso, S.; Baranov, D.; Giannini, C.; Marras, S.; Manna, L. Wide-Angle X-Ray Diffraction Evidence of Structural Coherence in $CsPbBr_3$ Nanocrystal Superlattices. *ACS Mater. Lett.* **2019**, *1*, 272−276.
(59) Ijaz, P.; Imran, M.; Soares, M. M.; Tolentino, H. C. N.; Martín-García, B.; Giannini, C.; Moreels, I.; Manna, L.; Krahne, R. Composition-, Size-, and Surface Functionalization-Dependent Optical Properties of Lead Bromide Perovskite Nanocrystals. *J. Phys. Chem. Lett.* **2020**, *11*, 2079−2085.

https://dx.doi.org/10.1021/acsnano.0c06595
ACS Nano 2021, 15, 650−664

(60) Nelson, C. A.; Zhu, X. Y. Reversible Surface Electronic Traps in PbS Quantum Dot Solids Induced by an Order-Disorder Phase Transition in Capping Molecules. *J. Am. Chem. Soc.* **2012**, *134*, 7592−7595.
(61) Butkus, J.; Vashishtha, P.; Chen, K.; Gallaher, J. K.; Prasad, S. K. K.; Metin, D. Z.; Laufersky, G.; Gaston, N.; Halpert, J. E.; Hodgkiss, J. M. The Evolution of Quantum Confinement in $CsPbBr_3$ Perovskite Nanocrystals. *Chem. Mater.* **2017**, *29*, 3644−3652.
(62) Ramade, J.; Andriambariarijaona, L. M.; Steinmetz, V.; Goubet, N.; Legrand, L.; Barisien, T.; Bernardot, F.; Testelin, C.; Lhuillier, E.; Bramati, A.; Chamarro, M. Fine Structure of Excitons and Electron-Hole Exchange Energy in Polymorphic $CsPbBr_3$ Single Nanocrystals. *Nanoscale* **2018**, *10*, 6393−6401.
(63) Kondo, S.-I.; Kakuchi, M.; Masaki, A.; Saito, T. Strongly Enhanced Free-Exciton Luminescence in Microcrystalline $CsPbBr_3$ Films. *J. Phys. Soc. Jpn.* **2003**, *72*, 1789−1791.
(64) Han, Q.; Wang, J.; Lu, J.; Sun, L.; Lyu, F.; Wang, H.; Chen, Z.; Wang, Z. Transition between Exciton-Polariton and Coherent Photonic Lasing in All-Inorganic Perovskite Microcuboid. *ACS Photonics* **2020**, *7*, 454−462.
(65) Stoumpos, C. C.; Malliakas, C. D.; Peters, J. A.; Liu, Z.; Sebastian, M.; Im, J.; Chasapis, T. C.; Wibowo, A. C.; Chung, D. Y.; Freeman, A. J.; Wessels, B. W.; Kanatzidis, M. G. Crystal Growth of the Perovskite Semiconductor $CsPbBr_3$: A New Material for High-Energy Radiation Detection. *Cryst. Growth Des.* **2013**, *13*, 2722−2727.
(66) Yang, R. X.; Tan, L. Z. Understanding Size Dependence of Phase Stability and Band Gap in $CsPbI_3$ Perovskite Nanocrystals. *J. Chem. Phys.* **2020**, *152*, 034702.
(67) Pan, J.; Li, X.; Gong, X.; Yin, J.; Zhou, D.; Sinatra, L.; Huang, R.; Liu, J.; Chen, J.; Dursun, I.; El-Zohry, A. M.; Saidaminov, M. I.; Sun, H.-T.; Mohammed, O. F.; Ye, C.; Sargent, E. H.; Bakr, O. M. Halogen Vacancies Enable Ligand-Assisted Self-Assembly of Perovskite Quantum Dots into Nanowires. *Angew. Chem., Int. Ed.* **2019**, *58*, 16077−16081.
(68) Liu, J.; Song, K.; Shin, Y.; Liu, X.; Chen, J.; Yao, K. X.; Pan, J.; Yang, C.; Yin, J.; Xu, L.-J.; Yang, H.; El-Zohry, A. M.; Xin, B.; Mitra, S.; Hedhili, M. N.; Roqan, I. S.; Mohammed, O. F.; Han, Y.; Bakr, O. M. Light-Induced Self-Assembly of Cubic $CsPbBr_3$ Perovskite Nanocrystals into Nanowires. *Chem. Mater.* **2019**, *31*, 6642−6649.
(69) Pan, L.; Ye, T.; Qin, C.; Zhou, B.; Lei, N.; Chen, S.; Yan, P.; Wang, X. α-$CsPbI_3$ Nanocrystals by Ultraviolet Light-Driven Oriented Attachment. *J. Phys. Chem. Lett.* **2020**, *11*, 913−919.
(70) Scheidt, R. A.; Atwell, C.; Kamat, P. V. Tracking Transformative Transitions: From $CsPbBr_3$ Nanocrystals to Bulk Perovskite Films. *ACS Mater. Lett.* **2019**, *1*, 8−13.
(71) Dang, Z.; Dhanabalan, B.; Castelli, A.; Dhall, R.; Bustillo, K. C.; Marchelli, D.; Spirito, D.; Petralanda, U.; Shamsi, J.; Manna, L.; Krahne, R.; Arciniegas, M. P. Temperature-Driven Transformation of $CsPbBr_3$ Nanoplatelets into Mosaic Nanotiles in Solution through Self-Assembly. *Nano Lett.* **2020**, *20*, 1808−1818.
(72) Bhaumik, S. Oriented Attachment of Perovskite Cesium Lead Bromide Nanocrystals. *ChemistrySelect* **2019**, *4*, 4538−4543.
(73) Sun, J.-K.; Huang, S.; Liu, X.-Z.; Xu, Q.; Zhang, Q.-H.; Jiang, W.-J.; Xue, D.-J.; Xu, J.-C.; Ma, J.-Y.; Ding, J.; Ge, Q.-Q.; Gu, L.; Fang, X.-H.; Zhong, H.-Z.; Hu, J.-S.; Wan, L.-J. Polar Solvent Induced Lattice Distortion of Cubic $CsPbI_3$ Nanocubes and Hierarchical Self-Assembly into Orthorhombic Single-Crystalline Nanowires. *J. Am. Chem. Soc.* **2018**, *140*, 11705−11715.
(74) Jeon, S.; Jung, M.-C.; Ahn, J.; Woo, H. K.; Bang, J.; Kim, D.; Lee, S. Y.; Woo, H. Y.; Jeon, J.; Han, M. J.; Paik, T.; Oh, S. J. Post-Synthetic Oriented Attachment of $CsPbBr_3$ Perovskite Nanocrystal Building Blocks: From First Principle Calculation to Experimental Demonstration of Size and Dimensionality (0D/1D/2D). *Nanoscale Horiz.* **2020**, *5*, 960−970.
(75) Pradhan, B.; Mushtaq, A.; Roy, D.; Sain, S.; Das, B.; Ghorai, U. K.; Pal, S. K.; Acharya, S. Postsynthesis Spontaneous Coalescence of Mixed-Halide Perovskite Nanocubes into Phase-Stable Single-Crystalline Uniform Luminescent Nanowires. *J. Phys. Chem. Lett.* **2019**, *10*, 1805−1812.
(76) Hudait, B.; Dutta, S. K.; Patra, A.; Nasipuri, D.; Pradhan, N. Facets Directed Connecting Perovskite Nanocrystals. *J. Am. Chem. Soc.* **2020**, *142*, 7207−7217.
(77) Schuller, I. K. New Class of Layered Materials. *Phys. Rev. Lett.* **1980**, *44*, 1597−1600.
(78) Lutz, H. D.; Beckenkamp, K.; Peter, S. Laurionite-Type M(OH)X (M = Ba, Pb; X = Cl, Br, I) and Sr(OH)I. An IR and Raman Spectroscopic Study. *Spectrochim. Acta, Part A* **1995**, *51*, 755−767.
(79) Lutz, H. D.; Beckenkamp, K.; Kellersohn, T.; Möller, H.; Peter, S. Neutron and X-Ray Structure Determination of Laurionite-Type Pb{O(H,D)}X, with X= Cl, Br, and I, Hydrogen Bonds to Lead(II) Ions as a Hydrogen-Bond Acceptor. *J. Solid State Chem.* **1996**, *124*, 155−161.
(80) Yu, Y.; Hou, J.; Zhang, L.; Sun, Q.; Attique, S.; Wang, W.; Xu, X.; Xu, F.; Ci, Z.; Cao, B.; Qiao, X.; Xiao, X.; Yang, S. Ultrastable Laurionite Spontaneously Encapsulates Reduced-Dimensional Lead Halide Perovskites. *Nano Lett.* **2020**, *20*, 2316−2325.
(81) Leon, F. R.; Zaitseva, N.; Gerion, D.; Huser, T.; Krol, D. Optical Properties of CdSe Nanoparticle Assemblies. *MRS Proceedings* **2003**, *789*, N11.13.
(82) Zaitseva, N.; Manna, L.; Gerion, D.; Saw, C. K. Precipitation of Selenium from CdSe Nanocrystal Solutions. *Adv. Mater.* **2005**, *17*, 1321−1324.
(83) Zaitseva, N.; Dai, Z. R.; Leon, F. R.; Krol, D. Optical Properties of CdSe Superlattices. *J. Am. Chem. Soc.* **2005**, *127*, 10221−10226.
(84) Burnham, D. C.; Chiao, R. Y. Coherent Resonance Fluorescence Excited by Short Light Pulses. *Phys. Rev.* **1969**, *188*, 667−675.
(85) Schlaus, A. P.; Spencer, M. S.; Miyata, K.; Liu, F.; Wang, X.; Datta, I.; Lipson, M.; Pan, A.; Zhu, X. Y. How Lasing Happens in $CsPbBr_3$ Perovskite Nanowires. *Nat. Commun.* **2019**, *10*, 265.
(86) He, M.; Jiang, Y.; Liu, Q.; Luo, Z.; Ouyang, C.; Wang, X.; Zheng, W.; Braun, K.; Meixner, A. J.; Gao, T.; Wang, X.; Pan, A. Revealing Excitonic and Electron-Hole Plasma States in Stimulated Emission of Single $CsPbBr_3$ Nanowires at Room Temperature. *Phys. Rev. Appl.* **2020**, *13*, 044072.
(87) Nakamura, T.; Firdaus, K.; Adachi, S. Electron-Hole Plasma Lasing in a ZnO Random Laser. *Phys. Rev. B: Condens. Matter Mater. Phys.* **2012**, *86*, 205103.
(88) Mitsubori, S.; Katayama, I.; Lee, S. H.; Yao, T.; Takeda, J. Ultrafast Lasing Due to Electron-Hole Plasma in ZnO Nano-Multipods. *J. Phys.: Condens. Matter* **2009**, *21*, 064211.
(89) Crooker, S. A.; Hollingsworth, J. A.; Tretiak, S.; Klimov, V. I. Spectrally Resolved Dynamics of Energy Transfer in Quantum-Dot Assemblies: Towards Engineered Energy Flows in Artificial Materials. *Phys. Rev. Lett.* **2002**, *89*, 186802.
(90) Mork, A. J.; Weidman, M. C.; Prins, F.; Tisdale, W. A. Magnitude of the Förster Radius in Colloidal Quantum Dot Solids. *J. Phys. Chem. C* **2014**, *118*, 13920−13928.
(91) Lee, E. M. Y.; Tisdale, W. A.; Willard, A. P. Nonequilibrium Dynamics of Localized and Delocalized Excitons in Colloidal Quantum Dot Solids. *J. Vac. Sci. Technol., A* **2018**, *36*, 068501.
(92) Han, Q.; Wu, W.; Liu, W.; Yang, Q.; Yang, Y. Temperature-Dependent Photoluminescence of $CsPbX_3$ Nanocrystal Films. *J. Lumin.* **2018**, *198*, 350−356.
(93) de Weerd, C.; Gomez, L.; Zhang, H.; Buma, W. J.; Nedelcu, G.; Kovalenko, M. V.; Gregorkiewicz, T. Energy Transfer between Inorganic Perovskite Nanocrystals. *J. Phys. Chem. C* **2016**, *120*, 13310−13315.
(94) Förster, T. Intermolecular Energy Migration and Fluorescence. *Ann. Phys. (Berlin, Ger.)* **1948**, *437*, 55−75.
(95) Di Stasio, F.; Christodoulou, S.; Huo, N.; Konstantatos, G. Near-Unity Photoluminescence Quantum Yield in $CsPbBr_3$ Nanocrystal Solid-State Films *via* Postsynthesis Treatment with Lead Bromide. *Chem. Mater.* **2017**, *29*, 7663−7667.
(96) Zhao, M.; Shi, Y.; Dai, J.; Lian, J. Ellipsometric Study of the Complex Optical Constants of a $CsPbBr_3$ Perovskite Thin Film. *J. Mater. Chem. C* **2018**, *6*, 10450−10455.

https://dx.doi.org/10.1021/acsnano.0c06595
ACS Nano 2021, 15, 650−664

(97) Cerdán, L.; Enciso, E.; Martín, V.; Bañuelos, J.; López-Arbeloa, I.; Costela, A.; García-Moreno, I. FRET-Assisted Laser Emission in Colloidal Suspensions of Dye-Doped Latex Nanoparticles. *Nat. Photonics* **2012**, *6*, 621−626.
(98) Shen, T.-L.; Hu, H.-W.; Lin, W.-J.; Liao, Y.-M.; Chen, T.-P.; Liao, Y.-K.; Lin, T.-Y.; Chen, Y.-F. Coherent Förster Resonance Energy Transfer: A New Paradigm for Electrically Driven Quantum Dot Random Lasers. *Sci. Adv.* **2020**, *6*, No. eaba1705.
(99) Li, Y.; Wang, X.; Xue, W.; Wang, W.; Zhu, W.; Zhao, L. Highly Luminescent and Stable $CsPbBr_3$ Perovskite Quantum Dots Modified by Phosphine Ligands. *Nano Res.* **2019**, *12*, 785−789.
(100) Shamsi, J.; Kubicki, D.; Anaya, M.; Liu, Y.; Ji, K.; Frohna, K.; Grey, C. P.; Friend, R. H.; Stranks, S. D. Stable Hexylphosphonate-Capped Blue-Emitting Quantum-Confined $CsPbBr_3$ Nanoplatelets. *ACS Energy Lett.* **2020**, *5*, 1900−1907.
(101) Patra, B. K.; Agrawal, H.; Zheng, J. Y.; Zha, X.; Travesset, A.; Garnett, E. C. Close-Packed Ultrasmooth Self-Assembled Monolayer of $CsPbBr_3$ Perovskite Nanocubes. *ACS Appl. Mater. Interfaces* **2020**, *12*, 31764−31769.
(102) Nenon, D. P.; Pressler, K.; Kang, J.; Koscher, B. A.; Olshansky, J. H.; Osowiecki, W. T.; Koc, M. A.; Wang, L.-W.; Alivisatos, A. P. Design Principles for Trap-Free $CsPbX_3$ Nanocrystals: Enumerating and Eliminating Surface Halide Vacancies with Softer Lewis Bases. *J. Am. Chem. Soc.* **2018**, *140*, 17760−17772.
(103) Proppe, A. H.; Elkins, M. H.; Voznyy, O.; Pensack, R. D.; Zapata, F.; Besteiro, L. V.; Quan, L. N.; Quintero-Bermudez, R.; Todorovic, P.; Kelley, S. O.; Govorov, A. O.; Gray, S. K.; Infante, I.; Sargent, E. H.; Scholes, G. D. Spectrally Resolved Ultrafast Exciton Transfer in Mixed Perovskite Quantum Wells. *J. Phys. Chem. Lett.* **2019**, *10*, 419−426.
(104) Yettapu, G. R.; Talukdar, D.; Sarkar, S.; Swarnkar, A.; Nag, A.; Ghosh, P.; Mandal, P. Terahertz Conductivity within Colloidal $CsPbBr_3$ Perovskite Nanocrystals: Remarkably High Carrier Mobilities and Large Diffusion Lengths. *Nano Lett.* **2016**, *16*, 4838−4848.
(105) Sharma, D. K.; Hirata, S.; Vacha, M. Energy Localization *vs.* Charge Funneling in Aggregates of $CsPbBr_3$ Perovskite Nanocrystals. *J. Lumin.* **2020**, *222*, 117119.
(106) Daskalakis, K. S.; Maier, S. A.; Kéna-Cohen, S. Spatial Coherence and Stability in a Disordered Organic Polariton Condensate. *Phys. Rev. Lett.* **2015**, *115*, 035301.
(107) Caputo, D.; Ballarini, D.; Dagvadorj, G.; Sánchez Muñoz, C.; De Giorgi, M.; Dominici, L.; West, K.; Pfeiffer, L. N.; Gigli, G.; Laussy, F. P.; Szymańska, M. H.; Sanvitto, D. Topological Order and Thermal Equilibrium in Polariton Condensates. *Nat. Mater.* **2018**, *17*, 145−151.
(108) Giannozzi, P.; Andreussi, O.; Brumme, T.; Bunau, O.; Buongiorno Nardelli, M.; Calandra, M.; Car, R.; Cavazzoni, C.; Ceresoli, D.; Cococcioni, M.; Colonna, N.; Carnimeo, I.; Dal Corso, A.; de Gironcoli, S.; Delugas, P.; DiStasio, R. A.; Ferretti, A.; Floris, A.; Fratesi, G.; Fugallo, G.; et al. Advanced Capabilities for Materials Modelling with Quantum ESPRESSO. *J. Phys.: Condens. Matter* **2017**, *29*, 465901.
(109) Giannozzi, P.; Baroni, S.; Bonini, N.; Calandra, M.; Car, R.; Cavazzoni, C.; Ceresoli, D.; Chiarotti, G. L.; Cococcioni, M.; Dabo, I.; Dal Corso, A.; de Gironcoli, S.; Fabris, S.; Fratesi, G.; Gebauer, R.; Gerstmann, U.; Gougoussis, C.; Kokalj, A.; Lazzeri, M.; Martin-Samos, L.; et al. QUANTUM ESPRESSO: A Modular and Open-Source Software Project for Quantum Simulations of Materials. *J. Phys.: Condens. Matter* **2009**, *21*, 395502.
(110) Monkhorst, H. J.; Pack, J. D. Special Points for Brillouin-Zone Integrations. *Phys. Rev. B* **1976**, *13*, 5188−5192.
(111) Perdew, J. P.; Burke, K.; Ernzerhof, M. Generalized Gradient Approximation Made Simple. *Phys. Rev. Lett.* **1996**, *77*, 3865−3868.
(112) Perdew, J. P.; Burke, K.; Ernzerhof, M. Generalized Gradient Approximation Made Simple. *Phys. Rev. Lett.* **1997**, *78*, 1396−1396.
(113) Del Sole, R.; Girlanda, R. Optical Properties of Semiconductors within the Independent-Quasiparticle Approximation. *Phys. Rev. B: Condens. Matter Mater. Phys.* **1993**, *48*, 11789−11795.

https://dx.doi.org/10.1021/acsnano.0c06595
ACS Nano 2021, 15, 650−664